


Large-scale shell model study of β^- -decay properties of $N = 126$, 125 nuclei: Role of Gamow-Teller and first-forbidden transitions in the half-lives

Anil Kumar  and Noritaka Shimizu **Center for Computational Sciences, University of Tsukuba, Tennodai, Tsukuba 305-8577, Japan*Yutaka Utsuno *Advanced Science Research Center, Japan Atomic Energy Agency, Tokai, Ibaraki 319-1195, Japan and Center for Nuclear Study, The University of Tokyo, Hongo, Bunkyo-ku, Tokyo 113-0033, Japan*Cenxi Yuan *Sino-French Institute of Nuclear Engineering and Technology, Sun Yat-Sen University, Zhuhai, Guangdong 519082, China*Praveen C. Srivastava *Department of Physics, Indian Institute of Technology Roorkee, Roorkee 247667, India*

(Received 2 April 2024; revised 19 May 2024; accepted 3 June 2024; published 21 June 2024)

We investigate the β^- -decay properties of $N = 125$ and $N = 126$ isotones with $Z = 52-79$ through large-scale shell model calculations, considering both Gamow-Teller and first-forbidden transitions. We observed that the distributions of GT strength exhibit a prominent peak at lower excitation energies, making a substantial contribution to the resulting half-lives. This peak, dominated by the $\nu 0h_{9/2} \rightarrow \pi 0h_{11/2}$ transition, is enhanced on the proton-deficient side because the Pauli-blocking effect caused by the occupying the valence proton $0h_{11/2}$ orbit is weakened. It is also observed that the contributions of first-forbidden transitions are diminished with a decrease in proton number from $Z = 82$.

DOI: [10.1103/PhysRevC.109.064319](https://doi.org/10.1103/PhysRevC.109.064319)

I. INTRODUCTION

The β decay plays a pivotal role in astrophysical phenomena such as the rapid neutron capture process (r process). The r process is the most important mechanism for the synthesis of about half of the elements heavier than iron [1] and it occurs in an environment with relatively high temperatures ($T \approx 10^9$ K) and high neutron densities ($> 10^{20}$ neutrons/cm³) [2–6]. In the r process of explosive nucleosynthesis, the neutron capture rates decrease rapidly near the neutron shell closure at the magic neutron numbers $N = 50, 82$, and 126, and that time β decay becomes the dominant nuclear mechanism for driving the material to the heavier elements [7]. Therefore, the r process has to wait for several β processes to occur before further neutron captures are possible. As a consequence, the solar r -process abundance distribution path exhibits three maximum peaks at $A \approx 80, 130$, and 195, corresponding to the very-neutron-rich region of the nuclear chart with the magic neutron numbers $N = 50, 82$, and 126. These nuclei are called waiting point nuclei on the r -process path.

The abundances of the elements created by the r process are strongly dependent on several nuclear inputs like masses, neutron capture rates, photodisintegration, β -decay rates, β -delayed processes, as well as fission probabilities,

particularly at the waiting point nuclei. Among them, the β -decay processes of nuclei around the magic neutron numbers $N = 50, 82$, and 126 are liable for the flow of r process to the synthesise of heavier elements and for setting the r -process timescale [8]. On the experimental side, the β -decay half-lives of nuclei located in the vicinity of the magic neutron numbers $N = 50$ [9–12] and $N = 82$ [13–16] have been energetically measured. However, there is still a lack of experimental β -decay half-lives in the region around the r -process waiting-point nuclei at $N = 126$. Recently, Morales *et al.* [17] systematically measured β -decay half-lives of nineteen nuclei around doubly magic ^{208}Pb in the RISING project at GSI, which includes the study of the $N = 125$ nuclei such as ^{202}Ir , ^{203}Pt , and ^{204}Au and $N = 126$ nuclei such as ^{204}Pt and ^{205}Au . In the more recent study [18], twenty new experimental β -decay half-lives in the lead region have been reported. Notably, nine of these measurements were conducted for the first time, including the assessment of nuclei with neutron numbers $N = 125$ and $N = 126$. Exploring and studying new nuclei species in the vicinity of the heaviest neutron shell closure, particularly around $N = 126$, remains a persistent experimental challenge. The scenario is expected to be enhanced in the near future with the development of advanced technology in the experimental facilities. With the development of the radioactive ion-beam facilities of the new generation, several research programs are ongoing worldwide to investigate the *Terra Incognita* region near $N \approx 126$ nuclei below ^{208}Pb [7, 17, 19, 20].

*Contact author: shimizu@nucl.ph.tsukuba.ac.jp

Due to a lack of experimental information about the β -decay half-lives of waiting point nuclei at the third peak around $A \approx 195$ on the r -process path, the theoretical prediction of half-lives using nuclear models becomes more important. A lot of attention has been paid to calculations of β -decay properties relevant to r -process nuclei in the framework of the different nuclear models. Most of the half-life calculations involving $A \approx 195$ peak nuclei are done by the finite-range droplet model (FRDM) [21,22], FRDM-QRPA (quasiparticle random-phase approximation) [23], the Hartree-Fock-Bogoliubov(HFB)-QRPA [24,25], and density functional theory (DFT)-QRPA [8,26,27]. A new advanced method has been introduced, namely, the finite amplitude method (FAM)-QRPA, into the systematic β -decay studies [28,29]. Machine-learning techniques have also been employed to forecast β -decay half-lives [30]. More recently, a systematic study of even-even r -process waiting point nuclei with $N = 50, 82, 126,$ and 184 have been done based on the relativistic QRPA approaches, which is extended to include the quasiparticle-vibration coupling [31]. However, less attention has been paid to the shell model calculations of β -decay rates on $N = 126$ isotones. Early calculations included only Gamow-Teller (GT) transitions, which have been performed in Refs. [32,33]. However, in addition to GT transition, the role of first-forbidden (FF) transitions becomes decisive in determining the half-lives of waiting point nuclei around the third abundance peak [26]. Hereafter, the shell model calculations have been extended to incorporate the FF transitions and have been utilized to compute the half-lives for r -process nuclei in the vicinity of $N = 126$ shell closures with proton-rich side $Z = 64\text{--}78$ [34–36]. However, the model space in these shell model studies was severely restricted due to increasing the computational cost. Systematic shell model calculations have recently been performed to evaluate the various β -decay properties around ^{208}Pb [37,38]. Currently, the advent of computational resources offers the opportunity to conduct demanding large-scale calculations.

The present work aims to demonstrate the strength of GT transitions of $N = 126$ and $N = 125$ isotones as a function of decreasing the proton number from $Z = 79$ to $Z = 52$. This study found that the GT strengths in the low excitation energies are rather strong in the proton-deficient side due to the increasing number of proton holes in the $0h_{11/2}$, orbit, accelerating GT decay. It is also observed that the contributions of FF transitions are diminished on this side. Recently, the same scenario for $N = 82$ and 81 isotones have been observed in the strength of the GT transitions due to the increasing number of proton holes in the $0g_{9/2}$ orbit [39]. Here, we extend the previous shell model calculations on a large scale to evaluate the half-lives and β -delayed neutron emission probabilities by taking the effect of both the GT and FF transitions for waiting point nuclei. We performed the systematic shell model calculations to investigate the β -decay properties for $N = 125$ isotones. Our shell model predicted decay rates are found to be well consistent with the available experimental data. The present study of β -decay properties of waiting point nuclei around $A \approx 195$ will add more information in the third r -process abundance peak distributions.

This paper is organized as follows: Sec. II provides a layout of the theoretical framework for β decay, along with the description of the shell model valence space and its associated Hamiltonian. Sec. III provides an account of the β -decay half-lives, including the contributions of GT and FF transitions for very neutron-rich nuclei. Finally, Sec. IV summarizes the key findings of the present study.

II. METHOD

A. Beta decay theory

In our calculations of the decay rates, we take into account both GT and FF contributions. A detailed formalism for the β decay is well-established in the literature by Behrens and Bühring [40] (see also Ref. [41]). In this work, we have used a streamlined version of the formalism for the FF β^- -decay theory from Refs. [34,35,42]. The partial half-life of the β^- transition from the initial state of the parent nucleus to the final state of the daughter nucleus can be expressed as

$$t_{1/2} = \frac{\kappa}{f}, \quad (1)$$

where the constant $\kappa = 6144 \pm 2$ s [27,43] and the phase-space factor is written as

$$f = \int_1^{W_0} C(W)(W^2 - 1)^{1/2} W(W_0 - W)^2 F(Z, W) dW, \quad (2)$$

where W is the total energy of the emitted electron in units of electron mass and W_0 is the maximum energy of W . $F(Z, W)$ is the Fermi function. The factor $C(W)$ is the shape factor that contains all the nuclear structure information about β -decay transition. For GT transitions, the shape factor does not depend on electron energy, which has the form

$$C(W) = B(GT) = \frac{|\mathcal{M}_{GT}|^2}{2J_i + 1}, \quad (3)$$

where the J_i is the angular momentum of the initial state, and the \mathcal{M}_{GT} denotes the GT nuclear matrix elements, which is defined in Table I.

In the case of FF beta decay, the form of the shape factor $C(W)$ in Eq. (2) is evaluated as

$$C(W) = K_0 + K_1 W + K_{-1}/W + K_2 W^2, \quad (4)$$

where the coefficients K_n ($n = -1, 0, 1, 2$) depend on the FF nuclear matrix elements and are written as

$$\begin{aligned} \text{rank } 0 : K_{-1} &= -\frac{2}{3}\mu_1\gamma_1\zeta_0\mathcal{M}_0^S, \\ K_0 &= \zeta_0^2 + \frac{1}{9}(\mathcal{M}_0^S)^2, \end{aligned} \quad (5)$$

$$\begin{aligned} \text{rank } 1 : K_{-1} &= \frac{2}{3}\mu_1\gamma_1\zeta_1(x+u), \\ K_0 &= \zeta_1^2 + \frac{1}{9}(x+u)^2 - \frac{4}{9}\mu_1\gamma_1u(u+x) \\ &\quad + \frac{1}{18}W_0^2(2x+u)^2 - \frac{1}{18}\lambda_2(2x-u)^2, \\ K_1 &= -\frac{4}{3}uY - \frac{1}{9}W_0(4x^2+5u^2), \\ K_2 &= \frac{1}{18}[8u^2 + (2x+u)^2 + \lambda_2(2x-u)^2], \end{aligned} \quad (6)$$

TABLE I. Summary of GT and FF nuclear matrix elements, and where $\lambda = -g_A/g_V = 1.2701(25)$ [44] is the ratio of the axial-vector coupling constant to the vector coupling constant and additional factors can be defined as $C_1 = \sqrt{4\pi/3}Y_1$ and $C = 1/\sqrt{2J_i + 1}$.

Transition	Rank	Notations	Nuclear matrix element (NME)	NME in nonrelativistic approximation
GT	0	\mathcal{M}_{GT}	$\lambda \langle f \sigma t_- i \rangle$	
FF	0	\mathcal{M}_0^S	$\lambda \sqrt{3} \langle f ir [C_1 \otimes \sigma]^0 t_- i \rangle C$	
		\mathcal{M}_0^T	$\lambda \sqrt{3} \langle f \gamma_5 t_- i \rangle C$	$-\lambda \sqrt{3} \langle f (i/M_N) [\sigma \otimes \nabla]^0 t_- i \rangle C$
	1	x	$-\langle f ir C_1 t_- i \rangle C$	
		$\xi'y$	$-\langle f \alpha t_- i \rangle C$	$E_{\gamma x}$
	2	u	$\lambda \sqrt{2} \langle f ir [C_1 \otimes \sigma]^1 t_- i \rangle C$	
		z	$-2\lambda \langle f ir [C_1 \otimes \sigma]^2 t_- i \rangle C$	

$$\text{rank 2 : } K_0 = \frac{1}{12} z^2 (W_0^2 - \lambda_2),$$

$$K_1 = -\frac{1}{6} z^2 W_0,$$

$$K_2 = \frac{1}{12} z^2 (1 + \lambda_2), \quad (7)$$

with

$$\zeta_0 = V + \frac{1}{3} \mathcal{M}_0^S W_0, \quad V = \mathcal{M}_0^T + \xi \mathcal{M}_0^{S'}, \quad (8)$$

$$\zeta_1 = Y + \frac{1}{3} (u - x) W_0, \quad Y = \xi'y - \xi(u' + x'). \quad (9)$$

ξ and γ_1 are defined as $\xi = \alpha Z / (2R)$ and $\gamma_1 = [1 - (\alpha Z)^2]^{1/2}$ with α being the fine-structure constant and R is the charge radius for a uniform charge distribution. In this work, μ_1 and λ_2 are taken as the approximate values, $\mu_1 \approx 1$ and $\lambda_2 \approx 1$ [45]. The remaining quantities \mathcal{M}_0^S , \mathcal{M}_0^T , x , $\xi'y$, u , and z along with their primed values $\mathcal{M}_0^{S'}$, x' , and u' represent the nuclear matrix elements associated with the FF operators. The matrix elements without prime are presented in Table I. In addition, we need to calculate the primed matrix elements, which include the effect of spherical uniform charge distribution. The prime matrix elements are obtained by multiplying the operator with the factor of

$$1 - \frac{1}{5} \left(\frac{r}{R} \right)^2 \quad \text{for } 0 \leq r \leq R, \quad (10)$$

$$\frac{R}{r} - \frac{1}{5} \left(\frac{R}{r} \right)^3 \quad \text{for } R \leq r,$$

for the radial integral.

In this study, we have constrained the relativistic nuclear matrix element $\xi'y$ in terms of x matrix based on conserved vector current (CVC) theory in the following way [40,45]:

$$\xi'y = E_{\gamma x}, \quad (11)$$

where E_{γ} is the energy difference between the isobaric analog of the initial state and the final state, which is written as

$$E_{\gamma} = E_{\text{ias}(i)} - E_f = Q(\beta^-) + \Delta E_C - \delta m, \quad (12)$$

with $\delta m = (m_n - m_p - m_e)c^2 = 0.782$ MeV. $Q(\beta^-)$ is the β^- decay Q value, which plays a crucial role in estimating the half-lives since the phase-space factor is roughly proportional to Q^5 . $Q(\beta^-)$ can be written as

$$Q(\beta^-) = E_{\text{g.s.}}^{\text{par.}} - E_{\text{g.s.}}^{\text{dau.}} + \delta m, \quad (13)$$

and ΔE_C denotes the Coulomb displacement energy between isobaric-analog states and is estimated by the empirical

formula [35,46]

$$\Delta E_C = 1.4136(1) \tilde{Z} / A^{1/3} - 0.91338(11) \text{ MeV}, \quad (14)$$

with $\tilde{Z} = (Z_i + Z_f) / 2$.

To make a comparison between experiment and theory conveniently, we define the average shape factor as

$$\overline{C(W)} = f / f_0, \quad (15)$$

where f is defined in Eq. (2) and f_0 is

$$f_0 = \int_1^{W_0} (W^2 - 1)^{1/2} W (W_0 - W)^2 F_0(Z, W) dW, \quad (16)$$

where $F_0(Z, W)$ is the Fermi function, which considers the Coulomb interaction between the daughter nucleus and emitted β particles.

Utilizing all partial half-lives $t_{1/2}$ from Eq. (1) of the GT and FF decays, the total half-life $T_{1/2}$ is expressed as

$$\frac{1}{T_{1/2}} = \sum_f \frac{1}{t_{i \rightarrow f}}, \quad (17)$$

where f spans all the possible daughter states permitted to be populated through the GT and FF transitions.

To compute the β -delayed neutron emission probabilities P_n , we consider all β decays to daughter states f with energies above the one-neutron separations energy S_n as leading to neutron emission and it is obtained as

$$P_n = \left(\sum_{E_f \geq S_n} \frac{1}{t_{i \rightarrow f}} \right) / \left(\sum_{\text{all } f} \frac{1}{t_{i \rightarrow f}} \right). \quad (18)$$

B. Shell model framework

In this work, we have performed shell model calculations to evaluate the β -decay properties of $N = 126$ and $N = 125$ nuclei with proton numbers ranging from $Z = 52$ to $Z = 79$. The present study adopts a model space with proton number $50 \leq Z \leq 82$ by using $0g_{7/2}$, $1d_{5/2,3/2}$, $2s_{1/2}$, and $0h_{11/2}$ proton orbits and with neutron number $82 \leq N \leq 126$ by using the $0h_{9/2}$, $1f_{7/2,5/2}$, $2p_{3/2,1/2}$, and $0i_{13/2}$ neutron orbits. In the chosen model space, we have used the slightly modified effective Kuo-Herling Hamiltonian KHHE from Ref. [47], which has been constructed based on the hole-hole channel in a ^{208}Pb core. Earlier, the same model space and the original Kuo-Herling Hamiltonian KHHE from Refs. [48,49] have been used in the study of β decay by including GT and FF

transitions near to ^{208}Pb [34–36]. However, they have studied limited $N = 126$ nuclei with proton number $Z = 64$ –78 with the truncated model space. In this model space, the GT transitions are dominantly connected by the $\nu(0h_{9/2}) \rightarrow \pi(0h_{11/2})$ transition, whereas the FF transitions are connected by $\nu(0i_{13/2}) \rightarrow \pi(0h_{11/2})$ and $\nu(fp) \rightarrow \pi(sd)$ transitions. In this context, we employed the full model space to compute the GT and FF transitions in $N = 126$ isotones and GT transitions in $N = 125$ isotones. The full model space is also used for calculating the FF transitions in $N = 125$ isotones with $Z = 52$ –59 and $Z = 72$ –79. In practical calculations, we solved the eigenvalue problem of the shell model Hamiltonian matrix whose M -scheme dimension is 1.33×10^{10} at maximum. However, the dimension of the open-shell $N = 125$ nuclei surpasses this dimension, and the truncation of the model space is required.

Due to the limitation of computational resources, a monopole interaction-based truncation is applied to evaluate the FF transitions in the $N = 125$ isotones with $Z = 60$ –71. The monopole-based truncation has been previously used in Refs. [50,51]. Before discussing this truncation, we briefly mention the monopole Hamiltonian and the effective single-particle energy (ESPE), which play important roles in the shell model framework. The monopole Hamiltonian was defined to discuss the bulk properties of nuclei [52] and is often used to calculate the ESPE, which provides information about the varying shell structure [53,54]. The ESPE is defined as [50]

$$\mathcal{E}_j = \mathcal{E}_j^c + \sum_{j'} V_{m;jj'} N_{j'}, \quad (19)$$

where \mathcal{E}_j^c stands for the single-particle energy of the j single-particle orbit relative to core, and $N_{j'}$ represents the occupation number of j' orbit, and $V_{m;jj'}$ is the strength of the monopole interaction between two orbits j and j' . The detailed analysis employing the ESPE will be discussed later in Sec. III D.

The monopole-based truncation is realized utilizing the monopole part of the shell model interaction. The interacting shell model aims to build the wave function as a linear expansion of all possible antisymmetric Slater determinants within a particular model space, whereas the model space is commonly defined by taking in single-particle orbitals near the Fermi surface. Normally, the initial step in shell model calculations is to arrange the bases in terms of partitions, denoting a group of configurations with the same definite number of particles in each orbital [50]. Based on the evaluation of the ESPE, the total monopole energy of a given partition is estimated by

$$E_{\mathcal{P}}^m = \sum_j \mathcal{E}_j^c N_{\mathcal{P};j} + \sum_{j \leq j'} V_{m;jj'} \frac{N_{\mathcal{P};j}(N_{\mathcal{P};j} - \delta_{jj'})}{1 + \delta_{jj'}}, \quad (20)$$

where $N_{\mathcal{P};j}$ denotes the particle distribution of the j orbit in a given partition \mathcal{P} . One can arrange the order of all partitions based on the total monopole energy $E_{\mathcal{P}}^m$, and then we considered only the lowest monopole energy partitions up to a certain threshold energy, which is called the truncation energy hereafter. Since the final states of the β decays are dominantly covered by the low-lying excited states, it can be assumed that partition with a relatively high $E_{\mathcal{P}}^m$ would not make a

TABLE II. Quenching factors adopted in the present study in comparison to Zhi *et al.* [35] that define the effective operators. See the text for more details.

	GT	FF				
		M_0^S	M_0^T	x	u	z
Present	0.54	0.41	1.266	0.51	0.28	0.71
Ref. [35]		0.66	1.266	0.51	0.38	0.42

significant contribution to β -decay rates. This truncation method significantly reduces the computational dimension retaining the computational accuracy. The validity of this truncation scheme will be discussed in Sec. III A.

C. Effective operators

To make a comparison of the shell model calculated β -decay rate with the experimental one, we use effective operators in the calculations. In the case of GT transitions, the bare GT operator σt is substituted with an effective operator by multiplying a scaling factor q (a name coined as a quenching factor in several earlier studies), which can be written as $\hat{O}_{\text{GT}}^{\text{eff}} = q \sigma t$ [55–57]. A detailed analysis of the quenching factor of the GT operator in various mass regions of the nuclear chart was investigated in Ref. [58]. This investigation observed that substantial quenching in the GT operator within the shell model framework is necessary as the nuclear mass increases. Due to insufficient experimental information on GT transitions in the lead region, accurately determining the quenching factor for the GT operator is a challenging topic for nuclear physics. To address the quenching factor in GT transitions in this study, we adopt two experimentally known β^- transitions, namely, $^{199}\text{Pt}(5/2^-) \rightarrow ^{199}\text{Au}(7/2^-)$ and $^{200}\text{Au}^m(12^-) \rightarrow ^{199}\text{Au}(11^-)$, where full shell model calculations are possible in the model space. The quenching factor is determined by minimizing the chi-squared function for the theoretical M_{GT} values corresponding to experimental M_{GT} values. The obtained quenching factor for the GT operator is presented in Table II. In Ref. [58], a correlation for the effective axial-vector coupling constant dependent on atomic mass was determined as $g_A^{\text{eff}} = 1.269A^{-0.12}$ within the shell model framework. Notably, the calculated quenching factor for the atomic mass region around $A = 200$ is 0.53, aligning closely with the presently calculated quenching factor value of 0.54. Using this quenching factor, the obtained GT matrix elements and $\log f_0 t$ are reasonably agreed with the experimental data (see Table III).

The previous studies [35,49,61,62] show that the operators of rank 0, 1, and 2 in the FF β decay also required a quenching factor. To determine the quenching factor for each operator individually for used effective interaction in the chosen model space, we implemented shell model calculations for experimentally observed β -decay nuclei with neutron number $N = 125$ and $N = 126$. In this study, we selected a comparable set of FF transitions for nuclei similar to previous investigations [35,63] in the lead region. Additionally, we included two new FF transitions from the $1/2^-$ ground state of

TABLE III. Calculated Gamow-Teller matrix elements for the available experimental known allowed β^- -decay with and without obtained quenching factor. Also, compared the calculated $\log f_0 t$ values with experimental data [59,60].

Transition	$ \mathcal{M}_{\text{GT}} $			$\log f_0 t$		
	Expt.	SM ($q = 1$)	SM ($q = 0.54$)	Expt.	SM ($q = 1$)	SM ($q = 0.54$)
$^{199}\text{Pt}(5/2^-) \rightarrow ^{199}\text{Au}(7/2^-)$	0.114	0.297	0.160	6.45(1)	5.62	6.16
$^{200}\text{Au}^m(12^-) \rightarrow ^{200}\text{Hg}(11^-)$	0.349	0.608	0.327	6.1(3)	5.6	6.2

^{205}Hg to the $1/2_3^+$ and $3/2_3^+$ excited states of ^{205}Tl . To obtain quenching factors for all FF operators, we have minimized the chi-squared function between theoretical and experimental average shape factors. However, the present set contains two FF unique transitions, namely, $^{205}\text{Hg}(\frac{1}{2}^-) \rightarrow ^{205}\text{Tl}(\frac{5}{2}_1^+)$ and $^{206}\text{Tl}(0^-) \rightarrow ^{206}\text{Pb}(2_1^+)$ (see Table IV). Therefore, we have calculated the square root of the average shape factor of unique and nonunique β decays in the same manner. To bring the unique transitions on equal footing to nonunique transitions in minimization at the same time, we have used the quantity $f_0 t_{1/2}$ to calculate the average shape factor from the experimental side, obtained by the experimental partial half-life $t_{1/2}$ with the calculated phase-space factor f_0 instead of the uniquely treated quantity $f_1 t_{1/2}$ with the unique β -decay phase-space factor f_1 values [64]. Additionally, we utilized two ways to determine the quenching factor of the rank-2 operator q_z . First, the quenching factor q_z is determined separately only for two unique FF transitions. Second, it is

determined by including both unique and nonunique transitions (two unique and sixteen nonunique transitions) simultaneously. The obtained quenching factors q_z in these two ways are the same, indicating the small contributions of the rank-2 operator in nonunique β decays.

A summary of the quenching factors we adopt for the GT and FF matrix elements is shown in Table II. The obtained quenching factors for the FF operators are found to be close to the previous shell model study of $N = 82$ and 126 isotones [35] except for rank-2 quenching factor q_z in the unique FF transitions. This is because we are presently utilizing the unique treatment in the FF unique transitions, as suggested by Warburton *et al.* [45]. The calculated partial half-lives and average shape factors, obtained by the shell model and the experimental $Q(\beta^-)$ values for the FF transitions using optimal quenching factors from Table II are presented in Table IV. Moreover, square root values of the shell model average shape factors compared with experimental data are shown in Fig. 1.

TABLE IV. Theoretical decay rates for experimentally known beta-decay transitions for $N = 125, 126$ isotones with the present quenching factors. Experimental data are taken from Refs. [65–69].

Transition		Q		$\log f_0 t$			$(\overline{C(W)})^{1/2}$ (fm)		
				Theory		Expt.	Theory		Expt.
Initial	Final	SM	Expt.	Q_{SM}	$Q_{\text{Expt.}}$		Q_{SM}	$Q_{\text{Expt.}}$	
$^{205}\text{Hg}(\frac{1}{2}^-)$	$^{205}\text{Tl}(\frac{1}{2}_1^+)$	1.614	1.533 (4)	5.320	5.320	5.257 (11)	66.21	66.21	71.2 (9)
	$^{205}\text{Tl}(\frac{1}{2}_2^+)$	0.463	0.314 (4)	6.797	6.796	7.03 (25)	12.09	12.10	9 (3)
	$^{205}\text{Tl}(\frac{1}{2}_3^+)$	0.248	0.099 (4)	5.919	5.919	5.6 (3)	33.21	33.24	48 (16)
	$^{205}\text{Tl}(\frac{3}{2}_1^+)$	1.432	1.329 (4)	6.455	6.463	6.51 (21)	17.93	17.77	17 (4)
	$^{205}\text{Tl}(\frac{3}{2}_2^+)$	0.506	0.392 (4)	7.048	7.057	7.65 (22)	9.06	8.96	5 (1)
	$^{205}\text{Tl}(\frac{3}{2}_3^+)$	0.292	0.193 (4)	6.548	6.557	6.43 (22)	16.10	15.94	18 (5)
	$^{205}\text{Tl}(\frac{5}{2}_1^+)$	0.910	0.914 (4)	7.942	7.939	8.29 (22)	3.24	3.25	2.2(5)
$^{206}\text{Tl}(0^-)$	$^{206}\text{Pb}(0_1^+)$	1.523	1.5323 (6)	5.176	5.176	5.1775 (13)	78.16	78.14	78.0 (1)
	$^{206}\text{Pb}(0_2^+)$	0.367	0.3659 (6)	5.630	5.630	5.99 (6)	46.32	46.32	31 (2)
	$^{206}\text{Pb}(2_1^+)$	0.717	0.7293 (6)	8.343	8.332	8.32 (3)	2.038	2.07	2.09(7)
$^{205}\text{Au}(\frac{3}{2}^+)$	$^{205}\text{Hg}(\frac{1}{2}_1^-)$	3.201	3.520	6.769	6.747	5.79 (9)	12.49	12.81	39 (4)
	$^{205}\text{Hg}(\frac{3}{2}_1^-)$	2.749	3.053	7.997	7.978	6.43 (11)	3.04	3.11	18 (2)
	$^{205}\text{Hg}(\frac{5}{2}_1^-)$	2.850	3.141	6.014	6.002	6.37 (12)	29.81	30.18	20 (3)
$^{206}\text{Hg}(0^+)$	$^{206}\text{Tl}(0_1^-)$	1.371	1.308 (20)	5.073	5.071	5.41 (6)	88.01	88.15	60 (4)
	$^{206}\text{Tl}(1_1^-)$	1.073	1.003 (20)	5.362	5.363	5.24 (10)	63.12	63.02	73 (8)
	$^{206}\text{Tl}(1_2^-)$	0.729	0.659 (20)	5.849	5.853	5.67 (8)	36.01	35.86	44 (4)
$^{207}\text{Tl}(\frac{1}{2}^+)$	$^{207}\text{Pb}(\frac{1}{2}_1^-)$	1.417	1.418 (5)	5.087	5.087	5.108 (6)	86.59	86.59	84.5 (6)
	$^{207}\text{Pb}(\frac{3}{2}_1^-)$	0.519	0.520 (5)	6.149	6.149	6.157 (22)	25.50	25.50	25.3 (6)

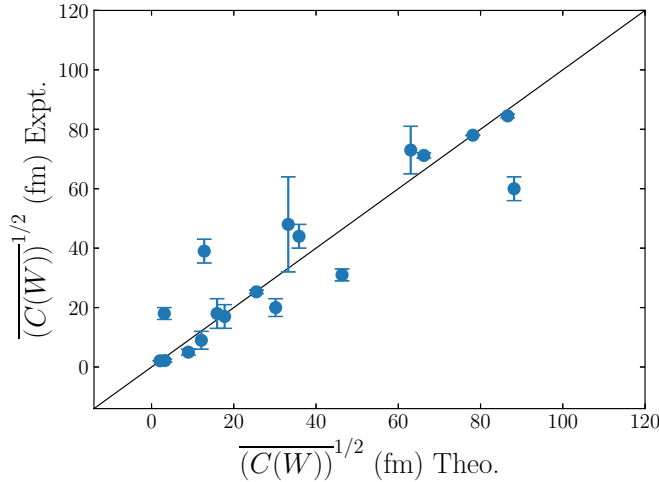


FIG. 1. Theoretical and experimental square root average shape factors for first-forbidden transitions with experimental Q values obtained using presently obtained quenching factor values from Table II.

In the case of the square root average shape factor, the matrix elements are multiplied by the electron Compton wavelength ($\tilde{\lambda}_{c_e} = 386.159$ fm), giving them a dimension of “fm”. A closer look reveals that the shell model decay rates for both $Q(\beta^-)$ values demonstrate good agreement with experimental values. In general, the shell model calculated average shape factors $\overline{C(W)}$ exhibit a good agreement with the experimental values within a factor of four, except for two decay cases in ^{205}Au . In these instances, the obtained average shape factor underestimates (the $1/2^-$ and $3/2^-$ states) from experimental results by approximately a factor larger than nine.

III. RESULTS

In this study, our primary interest is β -decay properties of nuclei near or on the neutron magic number $N = 126$. Hence, we have selected two isotonic chains with $N = 126$ and $N = 125$. Many of these nuclei reside on the r -process path, and their β -decay properties play a crucial role in determining the r -process path around the third peak. This section presents the computed results of low-lying energy spectra, $Q(\beta^-)$ values, β -decay half-lives, and β -delayed neutron emission probabilities of $N = 126$ and $N = 125$ isotones. We compare our calculated results with available experimental data and with two other nuclear models, namely, the FRDM and the KTUY model. All FRDM β -decay information is taken from the latest published paper [22]. In the case of KTUY, the $Q(\beta^-)$ values and other properties such as half-lives and β -delayed neutron emission probabilities taken from Ref. [70] that were predicted using the gross theory of beta decay [71] with the KTUY mass formula [72]. Hereafter, we have labeled these models as FRDM19 and KTUY05, where the numbers represent the last two digits of the publication years.

A. Convergence of monopole-based truncation

The β -decay half-lives are evaluated by including the GT and the FF transitions. Here, the GT strengths have been calculated using the Lanczos strength function method [52,73,74], with 250 Lanczos iterations to confirm sufficiently converged results for $N = 126$ and $N = 125$ isotones. In this case, the truncation of the model space is not required. However, for FF β decay, we have not utilized the Lanczos strength functions method to calculate the strength because it involves six operators in decay rates. Therefore, the FF strength has been obtained by the diagonalization of the Hamiltonian. In practice, we have computed 50 eigenstates for each spin-parity in the daughter nuclei. For the case of daughter nuclei of $N = 125$ isotones, the dimension of the open shell $N = 124$ nuclei increases drastically. Due to this, the truncation of the model space becomes crucial to make calculations feasible. As discussed in Sec. II B, we have implemented monopole-based truncation only for FF transitions in $N = 125$ nuclei with Z ranging from 60 to 71. Here, we examine convergence in the half-lives with the used truncation only in the case of FF transitions since the truncation is adopted further only in FF transitions in the present study.

To discuss the convergence of the monopole-based truncation in the computation of half-lives, we chose three nuclei in which the FF β^- transitions contribute significantly to the total half-life, namely, ^{193}Ho , ^{196}Yb , and ^{198}Hf with $N = 126$, as examples. These nuclei have 5.18×10^8 , 1.47×10^8 , and 3.36×10^7 M -scheme dimensions, respectively, which are tractable by the exact calculation and are large enough to discuss the convergence. The M -scheme dimension decreases rapidly with decreasing the truncation energy, as illustrated in Fig. 2(a).

Figure 2(b) shows the convergence of the shell model results of the total FF half-lives as a function of the truncation energies. The half-lives were calculated in two ways: one way is to use the transition strength and the $Q(\beta^-)$ value both of which are given by the truncated shell model calculation, and the other way is to use the truncated result for the transition strength and the exact shell model $Q(\beta^-)$ values without truncation. The figure shows that the shell model FF half-lives converge slightly faster using the $Q(\beta^-)$ values with the truncated model space than those without truncation because of the cancellation between the underestimation of the energy and the overestimation of the strength. Therefore, we use truncated $Q(\beta^-)$ values in further FF β -decay half-life calculations performed in truncated model space. The 5 MeV truncation energy is slightly low in estimating appropriate total FF half-lives since the FF matrix elements are strongly affected, causing a modest change in the half-lives due to the missing configurations higher than 5 MeV. However, the truncated FF half-lives achieved convergence by increasing the truncation energy, and a good convergence was obtained with truncation energies at 10, 15, and 20 MeV for the truncated $Q(\beta^-)$ values. Figure 3 shows the calculated square root of the average shape factor as a function of the excitation energy of concerned daughter nuclei. As seen in Fig. 3, the almost FF strengths are distributed only at the low-energy region, around $E_x = 2$ –3 MeV. Therefore, the truncation energy of 10

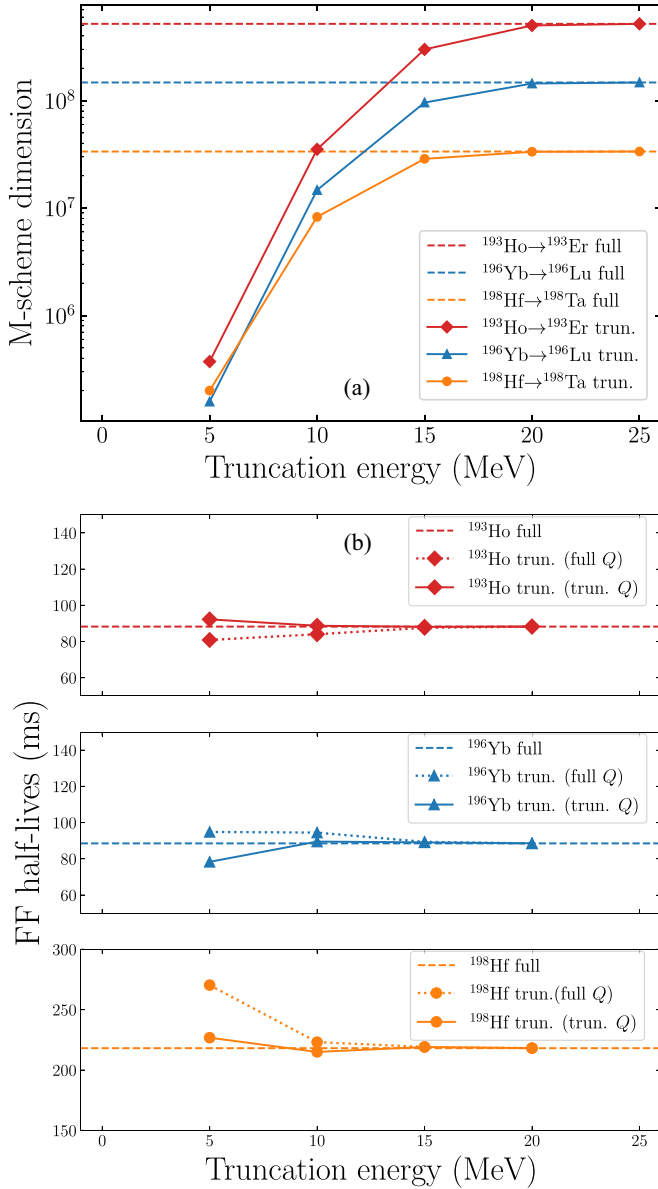


FIG. 2. (a) M -scheme dimensions of daughter nuclei against the truncation energy of the monopole-based truncation are plotted as the red diamonds (^{193}Ho), blue triangles (^{196}Yb), and orange circles (^{198}Hf) connected with the solid lines. The dimensions without truncation are shown as the dashed lines. (b) Shell-model first-forbidden half-lives of ^{193}Ho , ^{196}Yb , and ^{198}Hf against the truncation energy. The half-lives are evaluated using the shell model transition strength and $Q(\beta^-)$ values with the truncated model space (solid lines), and using the transition strength with the truncated model space and $Q(\beta^-)$ without the truncation (dotted lines). The exact shell model results without truncation are shown as dashed lines.

MeV is adequate to calculate the β -decay rate within the used model space. In the present study, we opted for a truncation energy of 10 MeV for subsequent calculations of FF transitions in $N = 125$ isotones with $Z = 60-71$. At this monopole truncation energy, the truncated calculated $Q(\beta^-)$ values were obtained within 0.5 MeV uncertainty from the full model space calculated $Q(\beta^-)$ values. This choice was motivated

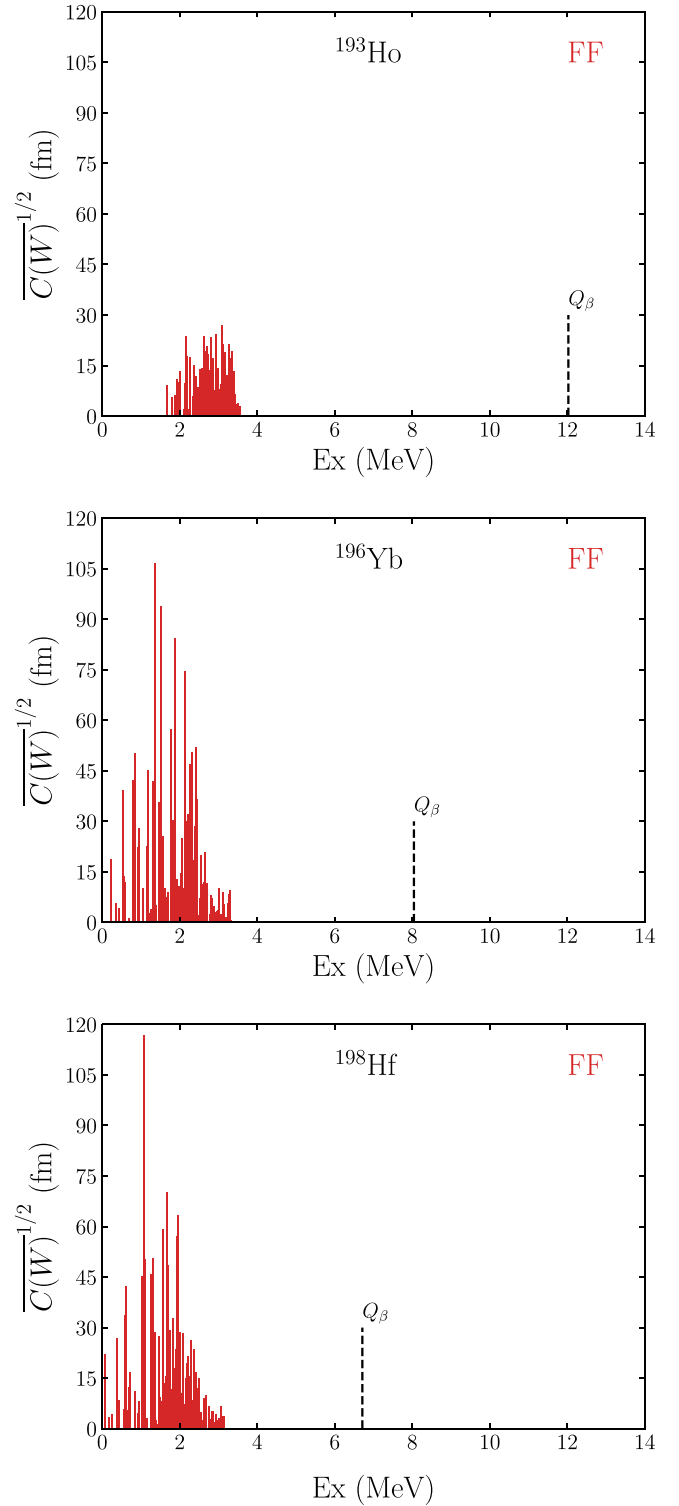


FIG. 3. Theoretical first-forbidden squared root of average shape factor for ^{193}Ho (top), ^{196}Yb (middle), and ^{198}Hf (bottom) are depicted as a function of excitation energies of the daughter nuclei.

by a significant reduction in the M -scheme dimensions at this truncation energy, rendering the shell model calculations more feasible.

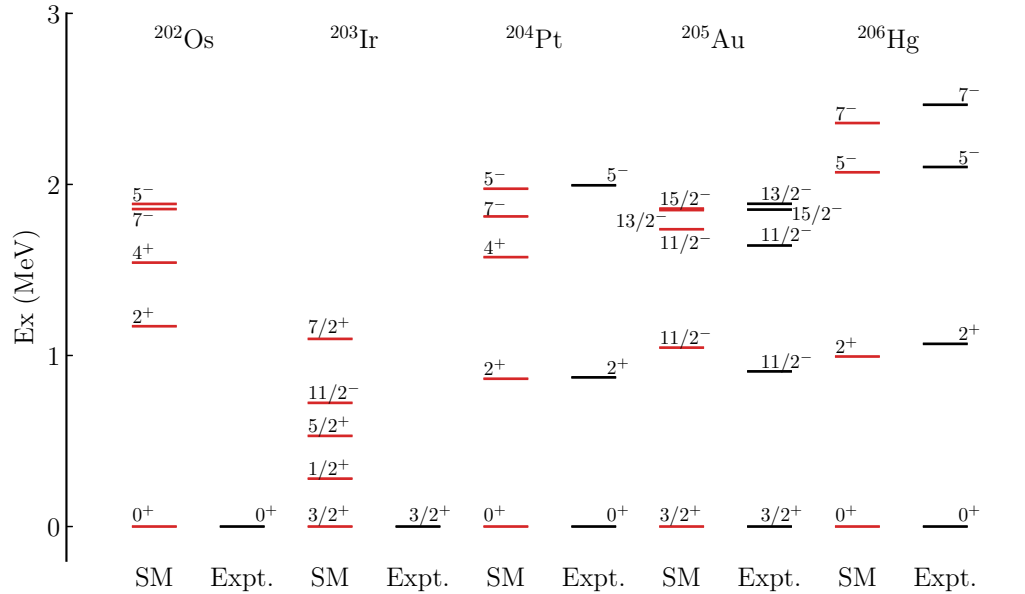


FIG. 4. Low-lying energy spectra of $N = 126$ isotones given by the present shell model result (SM) and the experimental data (Expt.) [75].

B. Low-lying energy spectra

The shell model Hamiltonian we adopted is based on the Kuo-Herling interaction, including the minor correction suggested in Yuan *et al.* [47], and its correction was validated by discussing the nuclear structures in the lead region. To confirm the validity of this interaction further, we have performed the shell model calculations for the ground and a few low-lying excited states of neutron-rich $N = 126$ and $N = 125$ nuclei with $Z = 76-81$ for which the experimental data are available, the results of which are shown in Figs. 4 and 5. As seen in Fig. 4, the ground-state spin-parities are correctly reproduced by the presently used interaction for all the $N = 126$

nuclei. The experimentally known excited states of $N = 126$ nuclei also reproduced reasonably. Figure 5 depicts the energy spectra of $N = 125$ isotones. The shell model successfully reproduces the experimental ground-state spin-parities except for ^{202}Ir and ^{204}Au . The ground state of ^{202}Ir is not confirmed from the experimental side. The shell model predicts a ground state with spin-parity 0^- and the first-excited state with spin-parity 2^- , lying only 27 keV higher. Concerning ^{204}Au , the shell model predicted ground state is 0^- , but the experimentally measured one is 2^- although the shell model predicted 2^- state is very close to the ground state, lying at 10 keV. The experimental excited states are still unknown for the cases of ^{201}Os and ^{202}Ir . Concerning β -decay properties,

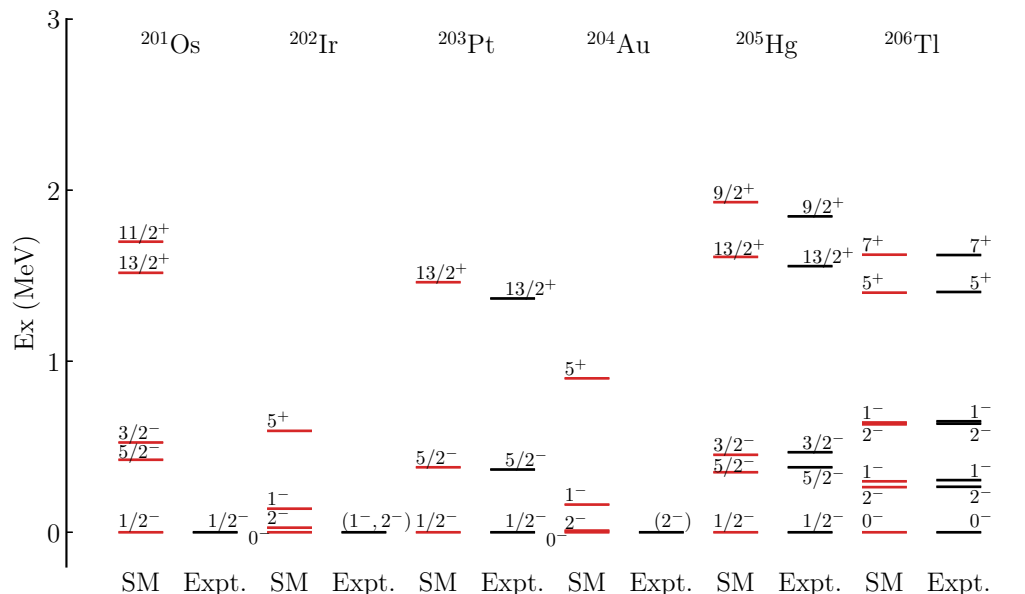


FIG. 5. Low-lying energy spectra of $N = 125$ isotones given by the present shell model result (SM) and the experimental data (Expt.) [75].

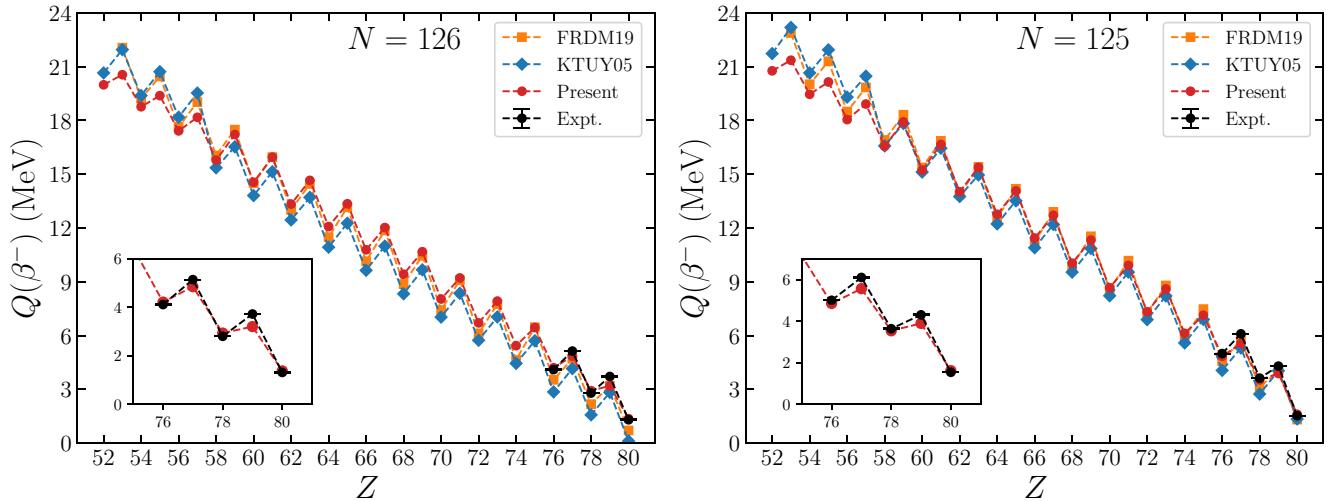


FIG. 6. Theoretical $Q(\beta^-)$ values for $N = 126$ (left panel) and $N = 125$ (right panel) isotones by the present shell model calculation (red circles), FRDM19 (orange squares) [22], and KTUY05 (blue diamonds) [71] in comparison with the existing experimental data (black circles with error bars) [75]. The inset only compared the present shell model calculated $Q(\beta^-)$ values with the known experimental data.

the involvement of the 0^- ground state and the 2^- and 1^- excited states in ^{202}Ir and ^{204}Au significantly contribute to the β -decay half-lives of ^{202}Os and ^{204}Pt , whose 0^+ ground state decays to the lowest 0^- , 1^- , and 2^- states most strongly with the FF transitions.

C. Half-lives of $N = 125$ and $N = 126$ isotones

The half-life is a fundamental property of radioactive nuclei that plays an important role in astrophysical phenomena, such as r -process nucleosynthesis [3]. Experimental data on $Q(\beta^-)$ for very neutron-rich $N = 126$ nuclei do not exist. Therefore, we derived $Q(\beta^-)$ values within the shell model framework and subsequently employed them in calculating half-lives. The calculated $Q(\beta^-)$ values of $N = 126$ and $N = 125$ isotones from the shell model are depicted in Fig. 6 and are compared with those from other nuclear models such as FRDM19 and KTUY05. The depicted $Q(\beta^-)$ values in the figures are calculated in the full model space. A comparison is also made with available experimental data near the $Z = 82$ side, $Z = 76$ – 80 . The $Q(\beta^-)$ values obtained from the shell model remarkably replicate the experimental values, exhibiting typical errors of less than 0.5 MeV. The odd-even staggering effect is also seen in the shell model calculated $Q(\beta^-)$ values, similar to that observed in the FRDM19 and KTUY05 models. Overall, the shell model $Q(\beta^-)$ values as a function of a decrease in proton number from $Z = 80$ to $Z = 52$ are demonstrating a consistent trend with the other theoretical models, FRDM19 and KTUY05, while slightly smaller values are predicated on the very proton-deficient side.

In the important r -process region near $Z = 60$ – 75 and $N = 126$, the significance of β -decay half-lives becomes crucial in determining the speed of matter flow and setting the r -process timescale. However, this region has limited experimental data for β -decay half-lives. To access the predictive capability

of our calculations, we first aim to reproduce the available experimental half-lives of $N = 126$ and $N = 125$ nuclei. For the case of $N = 126$ isotones, the β -decay half-life of ^{204}Pt and ^{205}Au has been measured in Ref. [17] and the obtained experimental half-life is 16_{-5}^{+6} s and 32.5(14) s, respectively. In a previous shell model study [36], the half-life given by using the original KHHE effective interaction in the same model space for ^{204}Pt is 38.3 s, which is the overestimation by a factor of 2.4. On the other hand, our current shell model half-life for ^{204}Pt is 13.9 s, which agrees with the experimental one within the experimental uncertainty. The shorter half-life in the present study compared with the previous one may be attributed to two reasons. First, the current investigation employed a modified KHHE Hamiltonian, leading to slightly larger $Q(\beta^-)$ values compared with the original Hamiltonian since the half-life is very sensitive to $Q(\beta^-)$; hence this difference can occur in the half-lives. In Ref. [47], the KHHE interaction has been modified by adding 0.1 MeV to all two-body matrix elements of proton-proton interaction except $\langle s_{1/2}s_{1/2} | V | s_{1/2}s_{1/2} \rangle$. This modification, as suggested by Yuan *et al.* [47], enhances the precision of binding energy. Therefore, the present obtained $Q(\beta^-)$ values from this modified KHHE interaction exhibit an excellent agreement between the calculated values from the shell model and the experimentally known data (see Fig. 6). Second, this discrepancy might be due to the different quenching scheme in FF operators, as the present study employed separate quenching factors for each operator.

Moreover, the new measurements of β -decay half-lives of three $N = 125$ nuclei such as ^{202}Ir , ^{203}Pt , and ^{204}Au have been made by Morales *et al.* [17]. For these nuclei, the present shell model predicted half-lives are underestimated by factors ranging from 1.1 to 2.4. A summary of the shell model β -decay half-lives in comparison to available experimental values is presented in Table V. This analysis also investigates the errors in the calculated β -decay half-lives relative

TABLE V. Comparison of the theoretical half-lives (s) of $N = 125$ and 126 nuclei with experimental data [17] and the previous shell model study.

	$N = 125$			$N = 126$	
	^{202}Ir	^{203}Pt	^{204}Au	^{204}Pt	^{205}Au
Present	4.7	20.6	25.4	13.9	23.7
Expt. [17]	15(3)	22(4)	37.2(8)	16_{-5}^{+6}	32.5(14)
SM 2018 [36]				38.3	

to experimentally known β -decay half-lives. It is important to note that we have analyzed the error just for the five experimental known β -decay transitions of $N = 126$ and $N = 125$ isotones. The directly calculated deviation between the theoretical and measured half-lives ($T_{1/2}^{\text{calc}} - T_{1/2}^{\text{expt}}$, where $T_{1/2}^{\text{calc}}$ and $T_{1/2}^{\text{expt}}$ signifying the respective shell model calculated and experimentally known half-lives) may not be suitable method due to two reasons. First, there are many order variations in the theoretically estimated half-lives. Second, there might be variations of many orders in the magnitude between the calculated and experimental half-lives. Therefore, these factors could amplify errors. Here, we have calculated the deviation and fluctuation in the half-life from experimental data based on the logarithm scale, following Refs. [23,42]. We introduce r as a measure of deviation

$$r = \log_{10} (T_{1/2}^{\text{calc}} / T_{1/2}^{\text{expt}}), \quad (21)$$

and its mean value and standard deviation can be written as

$$\bar{r} = \frac{1}{n} \sum_{i=1}^n r_i, \quad (22)$$

and

$$\sigma = \left[\frac{1}{n} \sum_{i=1}^n (r_i - \bar{r})^2 \right]^{1/2}, \quad (23)$$

respectively. The index i indicates a range from 1 to n , and n denotes the number of β -decay transitions used in the present error analysis. The terms \bar{r} and σ denote the mean deviation from the experimental data and the standard deviation expressed in terms of \log_{10} , respectively. Additionally, we expressed these values as $10^{\bar{r}}$ and 10^{σ} . In the ideal scenario, these values \bar{r} and σ would naturally be zero, or $10^{\bar{r}}$ and 10^{σ} being one would signify that all calculated results are identical to experimental values. Table VI displays the calculated quantities \bar{r} and σ along with their corresponding values $10^{\bar{r}}$ and 10^{σ} . Our obtained quantities \bar{r} and σ are -0.18 and 0.17 , respectively, which are approaching zero. The obtained value of $\sigma = 0.17$ or $10^{\sigma} = 1.48$ suggested that

TABLE VI. Discrepancies of shell model half-lives from the experimental ones. See main text for details.

\bar{r}	σ	$10^{\bar{r}}$	10^{σ}	n
-0.18	0.17	0.66	1.48	5

the present calculations accurately capture the characteristics of the β -strength function distribution. Overall, our calculated half-lives demonstrated good agreement benchmarks with the available experimental data.

As we move to the proton-deficient side, no experimental information about half-lives exists due to experimental difficulties. Nevertheless, we have performed systematic shell model calculations for the β -decay half-lives of $N = 126$ and $N = 125$ isotones with $Z = 52-79$. Figure 7 presents our shell model half-lives of $N = 126$ and $N = 125$ isotones with only GT transitions and with the inclusion of FF transitions in comparison with the experimentally available half-lives and other nuclear models FRDM19 and KTUY05 results. In the case of $N = 126$ isotone half-lives figure, we have also compared our shell model calculated half-lives with two previous shell model calculated half-life studies [35,36] in the same model space. In these earlier shell model studies, Suzuki *et al.* studied the half-lives of only $N = 126$ isotones with $Z = 64-78$ [36], Zhi *et al.* discussed the half-lives only for $N = 126$ nuclei with $Z = 66-73$ [35]. For comparison with other shell model results, we present only the half-lives in the present study and the earlier studies by Suzuki *et al.* [36] and Zhi *et al.* [35] for $N = 126$ isotones in Fig. 8. The present shell model half-lives demonstrate a similar trend to the earlier shell model results. However, note that the present half-lives are somewhat shorter than those of the other shell model results [35,36]. The difference would occur mostly due to the $Q(\beta^-)$ values since the half-life is very sensitive to the $Q(\beta^-)$ value. The present investigation adopted the modified KHHE Hamiltonian, which was marginally tuned to fit the available experimental binding energies [47] and gives slightly larger $Q(\beta^-)$ values than the original KHHE Hamiltonian as shown in Fig. 9. In addition, the previous studies used different quenching factors for the different multipole modes contributing to the decay rates. Furthermore, we performed the shell model calculations without truncating the model space of $N = 126$ isotones, while the other shell model studies applied severe particle-hole truncation to the model space. These several reasons make the present prediction of the half-lives shorter than the earlier studies.

In Fig. 7, the shell model studies do not predict the strong odd-even staggering in the half-lives as observed in the FRDM19 model at $Z > 70$, whereas the KTUY05-model predicted half-lives show a slight manifestation of this effect at $Z > 74$. The deviation in half-lives computed in this work compared with FRDM19 and KTUY05 are found to be less than approximately a factor of three to ten. However, our calculated half-lives trend reaches existing experimental half-lives at $Z = 78$ and 79 for $N = 126$ isotones and $Z = 77-79$ for $N = 125$ isotones. Our systematic findings of half-lives show a good agreement for $N = 126$ and $N = 125$ isotones among the different models. Next, the contribution of the FF transitions in the β -decay half-lives of the r -process waiting point nuclei raises a question about what extent and how these FF transitions become significant [7]. As already noted in Ref. [26], based on the DFT-QRPA, the importance of the FF transition becomes crucial in determining the half-lives of $N = 126$ r -process nuclei. This finding strongly supports the inclusion of FF transitions in our calculations. The

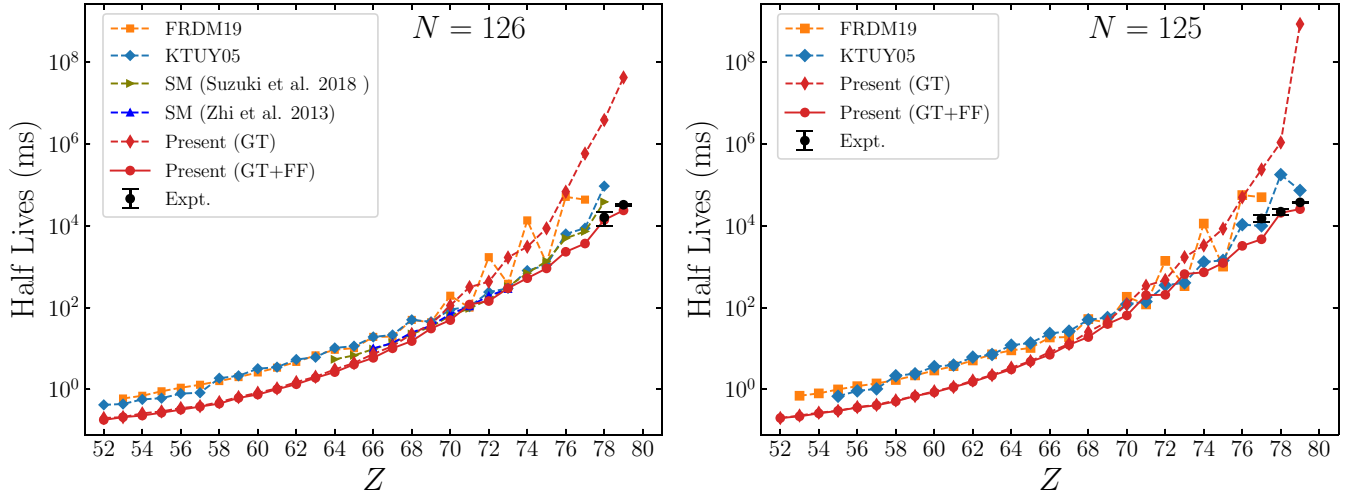


FIG. 7. Theoretical β -decay half-lives for $N = 126$ (left panel) and $N = 125$ (right panel) isotones by the present shell model calculation (red circles), FRDM19 (orange squares) [22], and KTUY05 (blue diamonds) [71] in comparison with the existing experimental data (black circles with error bars) [17]. The previous shell model studies are shown as brown right triangles [36] and blue triangles [35]. The half-lives given by the only GT transitions of the present shell model are also shown as red thin diamonds.

contributions of the GT and FF transitions in the half-lives of $N = 126$ isotones and $N = 125$ isotones with $Z = 52$ – 79 are depicted in Fig. 10, respectively. We observed an increased contribution of FF transitions with increased proton numbers towards $Z = 82$. The contributions of FF transitions in the total half-lives are expected to be enhanced around the third r -process abundance peak due to the attribute of the arrangement of the proton and neutron orbitals below ^{208}Pb in the employed model space. Since the model space in the present study consists of one-major-shell valence spaces, only the transition from the $\nu 0h_{9/2}$ orbital to the $\pi 0h_{11/2}$ orbital is allowed for the GT transition. As the proton number increases towards $Z = 82$, this transition becomes weakened due to occupying protons in the final $\pi 0h_{11/2}$ orbital and the location

of the $\nu 0h_{9/2}$ subshell is also hampered, which is the lowest lying neutron orbitals of the $82 < N < 126$ major shell [7]. A detailed discussion about the GT strengths is presented in Sec. III D. The present calculations predicted the contribution of the FF grows to approximate values from $\approx 3\%$ at $Z = 53$ to $\approx 100\%$ at $Z = 79$ as a function of increasing proton number. For the nuclei with proton number $Z \geq 70$ in $N = 126$ isotones and $Z \geq 72$ in $N = 125$ isotones, the contribution of FF transition becomes dominant in comparison to GT transitions in determining the half-lives. A strong odd-even staggering is also exhibited in the contributions of GT and FF transitions at $Z \leq 72$. The present analysis shows that the FF decay is dominant near $Z = 82$. Although this tendency previously has been demonstrated in various theoretical models [27,31], the

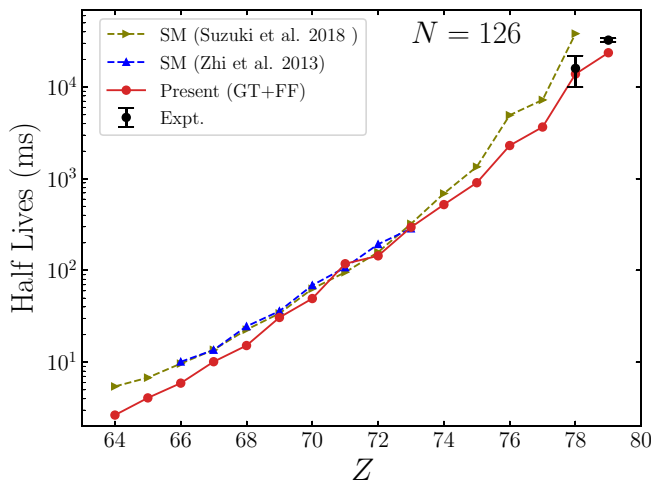


FIG. 8. Shell-model half-lives of the $N = 126$ isotones in the present study (red circles), by Suzuki *et al.* [36] (brown triangles) and Zhi *et al.* [35] (blue triangles). The existing experimental half-lives are shown as black circles with error bars.

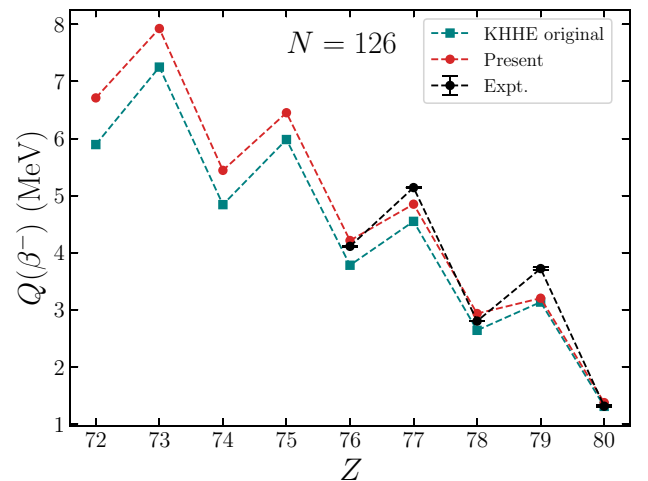


FIG. 9. Theoretical $Q(\beta^-)$ values for $N = 126$ isotones obtained by the modified KHHE Hamiltonian (red circles) in comparison to the original KHHE Hamiltonian (teal squares). The experimental $Q(\beta^-)$ values are shown as black circles with error bars.

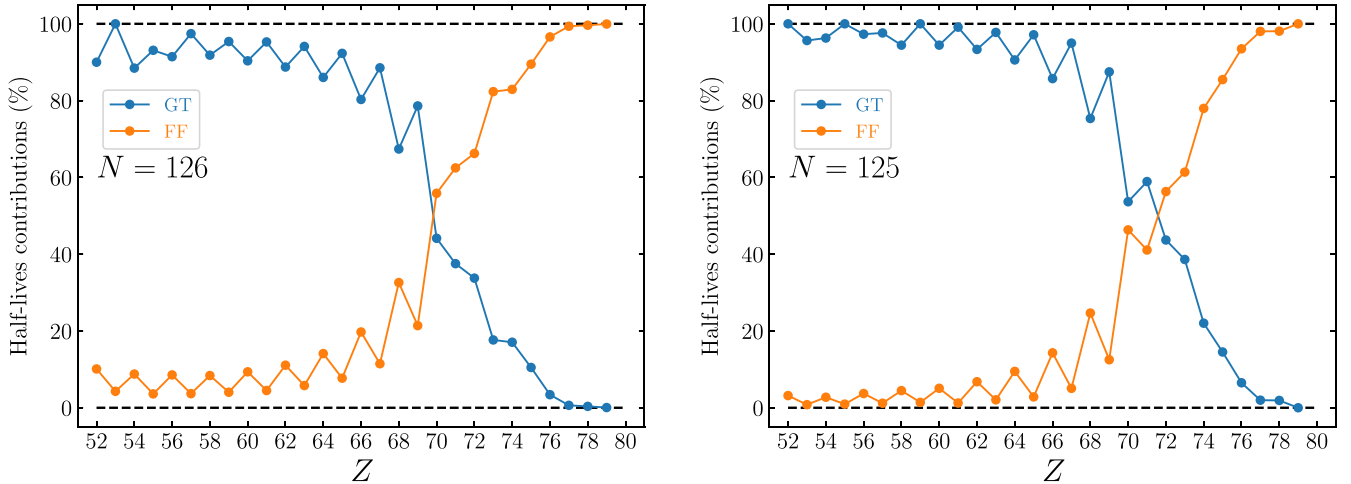


FIG. 10. Contributions of the Gamow-Teller (blue circles) and first-forbidden (orange circles) transitions in total half-lives of $N = 126$ (left panel) and $N = 125$ (right panel) isotones.

magnitude of the contributions varies from model to model. For example, in the study of $N = 126$ nuclei by Marketin *et al.* [27] employing the relativistic quasiparticle random-phase approximation (RQRPA), the predicted contribution of FF transitions undergoes a minor reduction from 90% at $Z = 73$ to 70% at $Z = 66$, while the present shell model predicts a stronger reduction from 82% at $Z = 73$ to reaching below 20% at $Z = 66$. The present study predicts smaller FF contributions on the proton-deficient side of the studied $N = 126$ isotonic chain than the other models such as RQRPA [27,31]. Further experimental data of the half-lives and Q values of the neutron-rich nuclei around the third peak of the r process are necessary to constrain the theoretical predictions.

β -delayed neutron emission probability is another measurable quantity that greatly impacts the r -process abundance of neutron-rich nuclei during the freeze-out process. This quantity influences the late-stage evolution by smoothing the odd-even staggering effect in the equilibrium pattern and providing neutrons during the freeze-out time [6]. Recently, β -delayed neutron emission probabilities in the neutron-rich Hg and Tl nuclei in the lead region have been measured in Ref. [18]. The behavior of presently calculated β -delayed neutron emission probabilities P_n for $N = 126$ isotones with $Z = 52$ –79 is shown in Fig. 11. In the present study, we assume the probability of β -decay to the states above the one neutron-emission threshold energy S_n is equal to P_n . As observed in Fig. 11, the P_n values are close to 100% in the $Z \leq 60$ region. This is attributed to small neutron-separation energies, around 1–2 MeV, and large $Q(\beta^-)$ values at $Z \leq 60$. In these isotones, the GT transition dominates the decay of these nuclei as seen in Fig. 10 and all GT distributions lie between the S_n and $Q(\beta^-)$ values as seen in Fig. 12. As the proton number increases at $62 \leq Z \leq 76$, the calculated P_n values decrease abruptly and strong odd-even staggering emerges simply due to the phase-space factor, similar to the previous shell model study [35]. Figure 11 further indicates that most of β decays go to states below neutron threshold energy for the case of even-even parent nuclei, yielding less P_n results as compared with near odd-even parent nuclei. However, no

experimental data on P_n at $N = 126$ region is available in the literature for comparison. In this context, we compare the calculated P_n results with those from the other theoretical nuclear models, FRDM19 and KTUY05. The KTUY05 result exhibits pronounced odd-even staggering and relatively smaller values than the shell model P_n results, while FRDM19 results show a weaker odd-even staggering and a trend similar to the present P_n results. Moreover, the present calculation predicted larger P_n values than most other calculations for the odd-even cases for $N = 126$ nuclei, primarily due to the more strength being distributed above the neutron-separation energy threshold.

D. Gamow-Teller strength function

As discussed in Sec. III C, the GT transitions become dominant in evaluating the half-lives on the proton-deficient side. The contribution of the GT transitions in the total half-lives

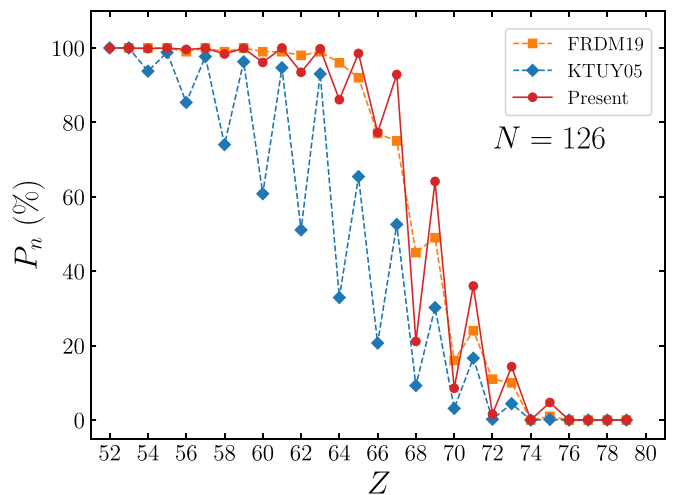


FIG. 11. Theoretical neutron emission probabilities $P_n(\%)$ of $N = 126$ isotones with varying proton numbers from $Z = 52$ to $Z = 78$ by the present shell model (red circles), FRDM19 (orange squares), and KTUY05 (blue diamonds).

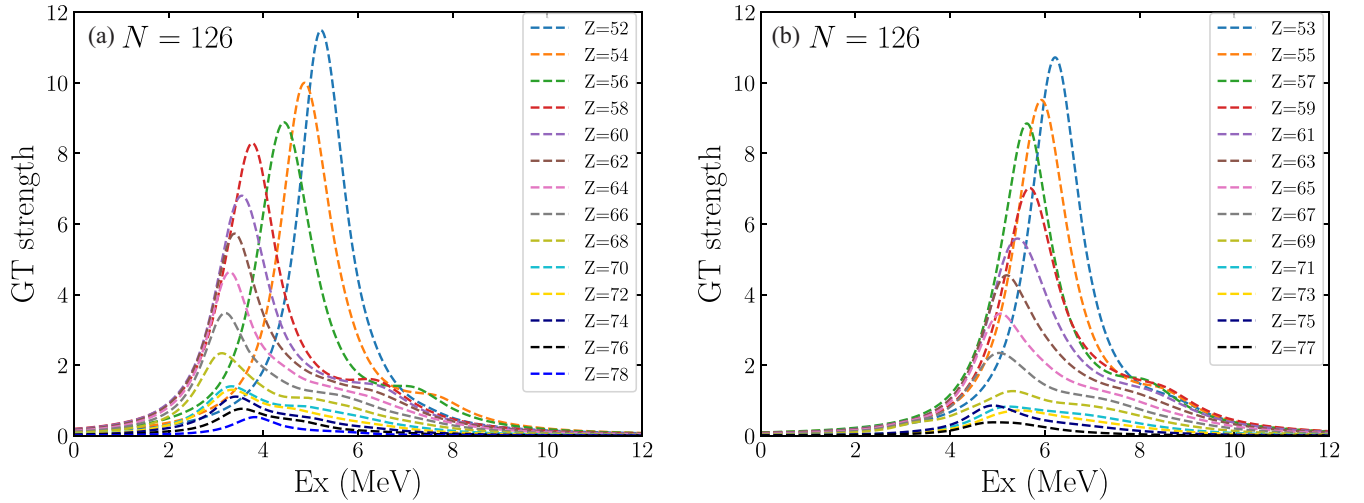


FIG. 12. Gamow-Teller strengths for $N = 126$ isotones for (a) even and (b) odd proton numbers are depicted as a function of excitation energies of the daughter nuclei. The strength function distribution is folded by a Lorentzian function with a width of 1 MeV. The values are presented without the quenching factor.

is illustrated in Fig. 10. Therefore, the extensive study of the GT transition also becomes important from the theory side. However, it is rather difficult to determine the GT strength from the experimental side. Figures 12 and 13 illustrated the presently calculated GT strength distribution as a function of the excitation energy of daughter nuclei with varying the proton number for $N = 126$ and $N = 125$ isotones, respectively. As we can see in these figures, the shell model calculated GT strengths exhibit a systematic distribution.

The present study made two most significant observations about the distribution of GT strengths. First, the GT strength occurs strongly at the low-excitation energies for $N = 126$ and $N = 125$ isotones. For the case of $N = 126$ isotones, the GT strength peaks are observed at low excitation energies between 3 and 6 MeV and 5 and 7 MeV for even Z and odd Z of parent nuclei, respectively (see in Fig. 12). In this observation, we find that the low-energy GT strength peaks obtained at a slightly higher energy for the odd- Z parents

are attributed to pairing correlation in daughter nuclei. By comparing the strength of the peaks between even Z and odd Z , we observe that even- Z isotopes have slightly stronger low-energy GT strength peaks than their neighboring odd- Z isotopes. The slight variation of these GT strengths peaks as a function of excitation energy corresponding to odd and even protons, reflects the influence of the odd-even effect in the sd - pf shell region, as noted in Ref. [42]. However, in the case of $N = 125$ isotones, these peaks exhibit a slight shift towards higher excitation compared with $N = 126$ isotones. Second, the GT strength peaks are systematically enhanced by decreasing the proton number from $Z = 79$ to $Z = 52$. In a recent shell model study [39], similar phenomena regarding Gamow-Teller strength were observed for $N = 82$ and $N = 81$ isotones. This observation coincided with a decrease in proton number, and the proton $0g_{9/2}$ orbit becomes unoccupied, similar to the proton $0h_{11/2}$ orbit in the present work. Here, we discuss the reason behind the phenomenon

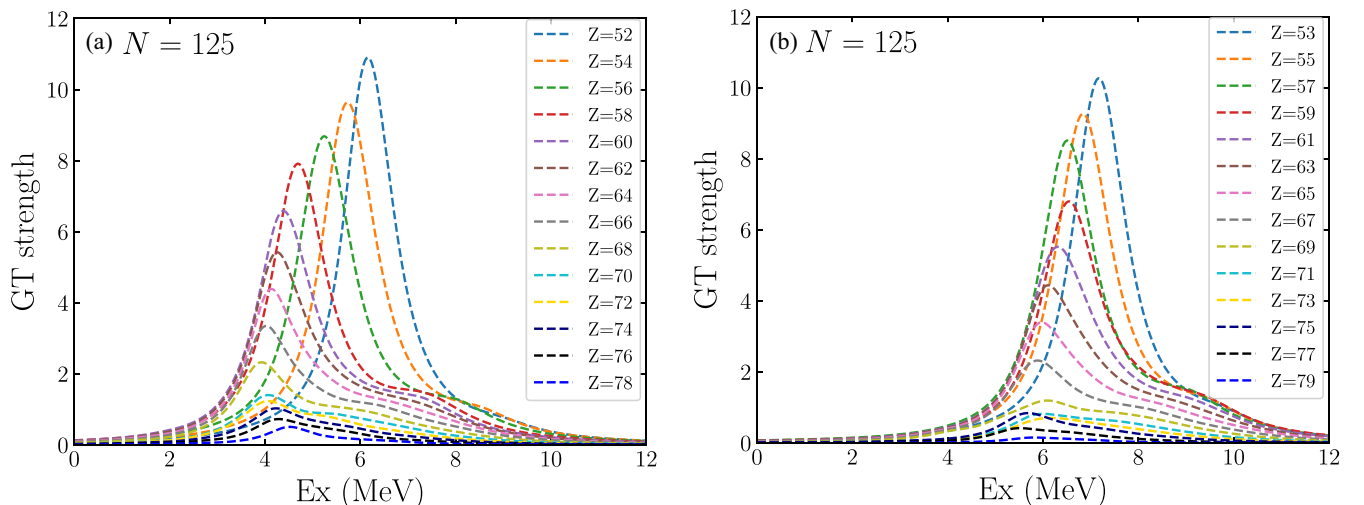


FIG. 13. Gamow-Teller strengths for $N = 125$ isotones. See the caption of Fig. 12 for details.

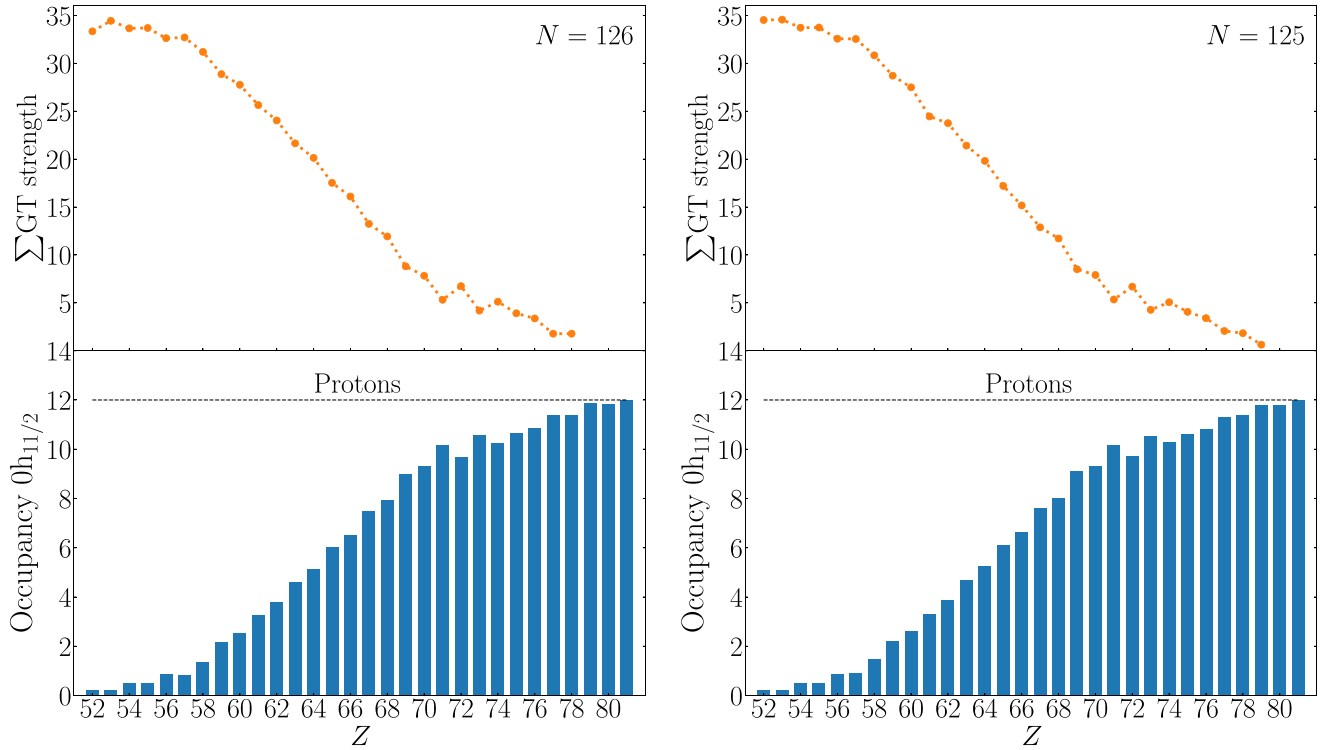


FIG. 14. Gamow-Teller sum rule (top) and occupancy of the $\pi 0h_{11/2}$ orbit (bottom) of the $N = 126$ (left) and $N = 125$ (right) isotones as a function of the proton number from $Z = 52$ to $Z = 81$.

of an enlarged peak with a decrease in Z . The low-energy GT strength peaks are governed by the $\nu 0h_{9/2} \rightarrow \pi 0h_{11/2}$ transition in the present model space. The proton number increases and occupies the $\pi 0h_{11/2}$ orbit, leading to a gradual Pauli blocking of the GT transitions. Figure 14 shows the total sum of GT strength as a function of proton occupancy in $\pi 0h_{11/2}$ orbit, varying the proton number for $N = 126$ and $N = 125$ isotones. It is evident from this figure that as the proton number increases, the proton $0h_{11/2}$ orbit becomes occupied, and simultaneously, the sum of GT strength decreases, reaching almost zero near $Z = 82$. Conversely, this effect can be diminished by removing the proton from $\pi 0h_{11/2}$ orbit, which enlarges the low-lying GT strength peak.

Concerning the sequences of single-particle levels, Fig. 15 illustrates the effective single-particle energies (ESPEs) of $N = 126$ isotones as a function of Z from the present Hamiltonian. In the previous study by part of the present authors [39], the evaluation of ESPEs for the case of $N = 82$ isotones with decreasing proton number from $Z = 50$ to $Z = 40$ revealed two notable findings. First, the neutron $0g_{7/2}$ orbit exhibited a significant shift in its position as Z decreased, reaching its second-highest orbit at $Z = 40$. Second, proton $0g_{9/2}$ orbit consistently maintained the lowest unoccupied orbit with this range. This phenomenon arises due to the central and tensor forces attracting cooperatively to generate a strong, attractive monopole interaction between $\pi 0g_{9/2}$ and $\nu 0g_{7/2}$ [76]. However, the ESPEs from $Z = 82$ to $Z = 70$ in the present study do not show a similar manner with the previous $N = 82$ study [39]. The depicted proton occupancy of the $\pi 0h_{11/2}$ orbit in Fig. 14 indicates that the proton occupied number

gradually changed between $Z \approx 55$ to $Z \approx 70$. At $Z \geq 71$ the $0h_{11/2}$ orbit is almost filled, reaching an occupancy of over 85%. In the $Z = 70$ – 82 region, the $2s_{1/2}$ and $1d_{3/2,5/2}$ orbitals play the lowest unoccupied orbital. The $2s_{1/2}$ and $1d_{3/2}$ orbitals occupy $\approx 12\%$ and $1d_{5/2}$ occupies $\approx 35\%$ at $Z = 70$, respectively. Most of FF transitions are connected by $\nu(0i_{13/2}) \rightarrow \pi(0h_{11/2})$, $\nu(0h_{9/2}) \rightarrow \pi(0g_{7/2})$, and $\nu(fp) \rightarrow \pi(sd)$ in the chosen model space. Hence, the FF transitions between $\nu(fp) \rightarrow \pi(sd)$ becomes important due to empty occupancy in $2s_{1/2}$ and $1d_{3/2}$ orbitals. As we have pointed out in Sec. III C the contribution of FF transitions becomes dominant over GT transitions at $Z \geq 70$ (see Fig. 10).

Hereafter, we briefly discuss the peak positions of the GT strength shown in Figs. 12 and 13. In a simple single-particle picture without the configuration-mixing effect, the peak energy can be understood in terms of the effective single-particle energies and two-body matrix elements of $\nu 0h_{9/2}$ and $\pi 0h_{11/2}$ orbits. Here, we chose one example of $N = 126$ nuclei with $Z = 52$ for this simple analysis; the low-energy GT strength peak emerges roughly at 5.2 MeV as shown in Fig. 12. According to the ESPEs in Fig. 15, the neutron $0h_{9/2}$ orbit lies roughly at 2.6 MeV below the Fermi surface at $Z = 52$, and the proton $0h_{11/2}$ orbit located ≈ 1.6 MeV above the Fermi surface. Since in nuclei close to $Z = 50$ protons occupy less than half filled in the $\pi 0h_{11/2}$ orbit and the GT transition creates a neutron $0h_{9/2}$ hole in the daughter states, the particle-hole matrix element $\langle \pi 0h_{11/2} (\nu 0h_{9/2})^{-1} | V | \pi 0h_{11/2} (\nu 0h_{9/2})^{-1} \rangle_{J=1}$ plays a dominant role. We present the shell model particle-hole matrix elements derived from hole-hole matrix elements using the Pandya transformation [77] of the concerned $\nu 0h_{9/2}$

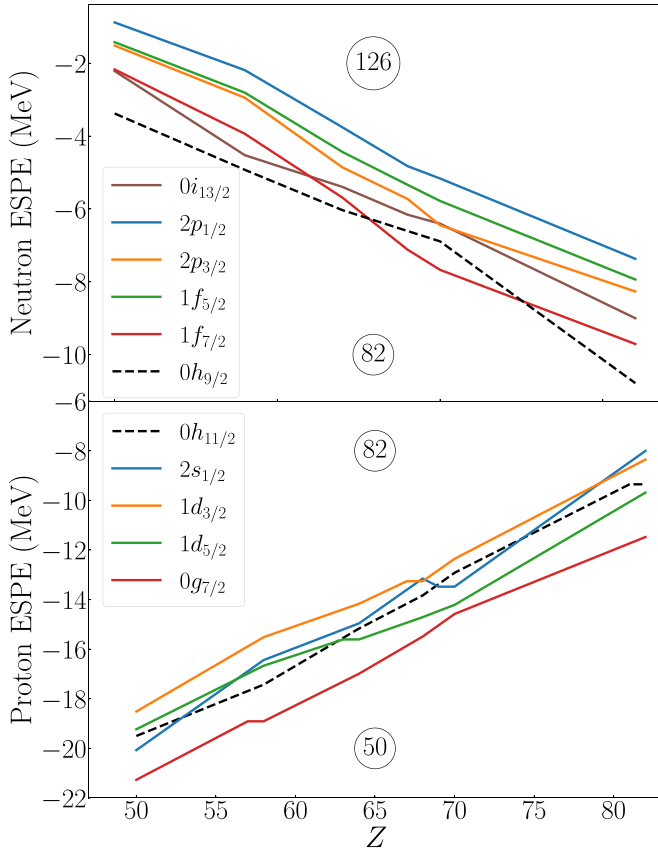


FIG. 15. Effective single-particle energies of the $N = 126$ isotones for neutron (top) and proton (bottom) orbits as a function of the proton number employing the modified KHHE interaction [47].

and $\pi 0h_{11/2}$ orbits in Fig. 16. This figure shows that the particle-hole matrix elements are repulsive for all the possible J values. The $J = 1$ coupled matrix element is most relevant to GT transitions and exhibits the largest positive value, 1.0 MeV stronger than the average monopole strength, thereby representing the largest contribution to the peak energy. A simple guess of the GT peak energy would be the sum of the neutron ESPE of the $\nu 0h_{9/2}$ orbit from the Fermi level, 2.6 MeV, the proton ESPE of the $\pi 0h_{11/2}$ orbit from the Fermi level, 1.6 MeV, and the particle-hole $J = 1$ matrix element, 1.0 MeV, causing 5.2 MeV and is consistent with the shell model result. In contrast, the peak energy of nuclei close to $Z = 82$ is dominated by the hole-hole matrix element $\langle (\pi 0h_{11/2})^{-1} (\nu 0h_{9/2})^{-1} | V | (\pi 0h_{11/2})^{-1} (\nu 0h_{9/2})^{-1} \rangle_J$, since the proton $0h_{11/2}$ orbit is almost occupied near the Fermi surface and the GT transition creates a neutron $0h_{9/2}$ hole in the daughter states. The hole-hole matrix elements of the $\nu 0h_{9/2}$ and $\pi 0h_{11/2}$ orbits are also shown in Fig. 16, which are attractive for all the possible J . Among them, the $J = 1$ coupled matrix element is relevant to the GT transition. Note that this J dependence is rather universal due to the parabolic rule that holds for short-range attractive forces [78]. Such a simple discussion does not work in the midshell nuclei due to the configuration-mixing effect and pairing correlations.

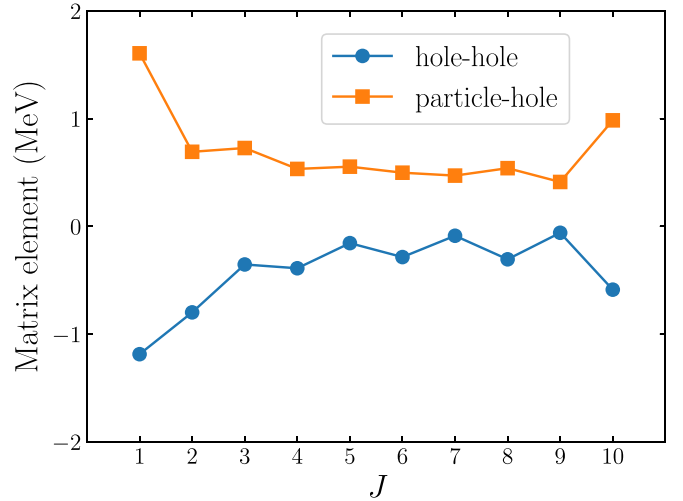


FIG. 16. Two-body diagonal Hamiltonian matrix elements of the $\pi 0h_{11/2}$ and $\nu 0h_{9/2}$ orbits in the modified KHHE interaction [47]. The elements of the hole-hole interaction, $\langle (\pi 0h_{11/2})^{-1} (\nu 0h_{9/2})^{-1} | V | (\pi 0h_{11/2})^{-1} (\nu 0h_{9/2})^{-1} \rangle_J$, and the elements of the particle-hole interaction, $\langle \pi 0h_{11/2} (\nu 0h_{9/2})^{-1} | V | \pi 0h_{11/2} (\nu 0h_{9/2})^{-1} \rangle_J$, are shown as the blue circles and orange squares, respectively.

IV. SUMMARY

We have investigated the nuclear β -decay properties such as half-lives and β -delayed neutron emission probabilities of $N = 126$ and $N = 125$ isotones with $Z = 52-79$. We performed the large-scale shell model calculations using the minor modified KHHE Hamiltonian with one major shell model space. To prove the validity of the interaction, we demonstrated that the shell model results of the low-lying energy spectra and $Q(\beta^-)$ value of neutron-rich $N = 126$, 125 nuclei reproduce the experimentally available data well. Additionally, we used the monopole-based truncation in the β -decay studies. Here, we have obtained a good convergence in the half-lives with this truncation. Thus, the monopole-based truncation allows us to perform large-scale shell model calculations for open-shell nuclei in heavier regions, in which the exact diagonalization is beyond the current computational limits. We have also investigated the β -decay properties of $N = 125$ isotones systematically in the shell model framework.

The present study considers the contributions of both the Gamow-Teller and the first-forbidden transitions in the β -decay rate. We have found that the first-forbidden contribution shortens the half-life at $Z \geq 70$ for $N = 126$, 125 isotones, demonstrating that the first-forbidden contribution is essential to estimating the total half-lives of these isotones. On the proton deficient side at $Z \leq 70$, the Gamow-Teller strength plays a dominant role in the half-lives. The low-energy Gamow-Teller strengths systematically grow with decreased protons number from $Z = 79$ to $Z = 52$ because the Pauli-blocking effect is weakened by the increased holes in the valence proton $0h_{11/2}$ orbit. Similarly, various other theoretical models also predict that the Gamow-Teller transition plays an important role in the proton deficient side, however, the predicted values

differ from each other quantitatively [27,31]. A possible future work is to investigate the origin of this difference.

In addition, we also found that the calculated total β -decay half-lives for $N = 126, 125$ nuclei showed a good agreement with the existing experimental data. Within our knowledge, no experimental data exist for half-lives below $Z < 78$ for $N = 126$ isotones and $Z < 77$ for $N = 125$ isotones. We have given a theoretical prediction of the half-lives for experimentally unknown β decay on the proton-deficient side, which would be useful for future experiments. The investigated systematic information of β -decay half-lives and β -delayed neutron emission probabilities will significantly impact our understanding of the r -process nucleosynthesis.

ACKNOWLEDGMENTS

A.K., N.S., and Y.U. acknowledge the support of the “Program for promoting research on the supercomputer Fugaku,” MEXT, Japan (JPMXP1020230411). C.Y. acknowledges the Guangdong Major Project of Basic and Applied Basic Research under Grant No. 2021B0301030006 and P.C.S. acknowledges a research grant from SERB (India), CRG/2022/005167. The shell model calculations were performed using the KSHELL code [79] mainly on the Fugaku supercomputer at R-CCS, RIKEN (hp230207), and the Pegasus supercomputer at the University of Tsukuba (MCRP program, NUCLSM and wo22i002).

-
- [1] E. M. Burbidge, G. R. Burbidge, W. A. Fowler, and F. Hoyle, Synthesis of the elements in stars, *Rev. Mod. Phys.* **29**, 547 (1957).
- [2] J. J. Cowan, F.-K. Thielemann, and J. W. Truran, The r -process and nucleochronology, *Phys. Rep.* **208**, 267 (1991).
- [3] T. Kajino, W. Aoki, A. Balantekin, R. Diehl, M. Famiano, and G. Mathews, Current status of r -process nucleosynthesis, *Prog. Part. Nucl. Phys.* **107**, 109 (2019).
- [4] J. J. Cowan, C. Sneden, J. E. Lawler, A. Aprahamian, M. Wiescher, K. Langanke, G. Martínez-Pinedo, and F.-K. Thielemann, Origin of the heaviest elements: The rapid neutron-capture process, *Rev. Mod. Phys.* **93**, 015002 (2021).
- [5] A. Arcones and F.-K. Thielemann, Origin of the elements, *Astron. Astrophys. Rev.* **31**, 1 (2023).
- [6] M. Mumpower, R. Surman, G. McLaughlin, and A. Aprahamian, The impact of individual nuclear properties on r -process nucleosynthesis, *Prog. Part. Nucl. Phys.* **86**, 86 (2016).
- [7] A. I. Morales, β -decay studies across $N = 126$, *J. Phys.: Conf. Ser.* **2586**, 012048 (2023).
- [8] I. Borzov, Beta-decay rates, *Nucl. Phys. A* **777**, 645 (2006).
- [9] M. Madurga, R. Surman, I. N. Borzov, R. Grzywacz, K. P. Rykaczewski, C. J. Gross, D. Miller, D. W. Stracener, J. C. Batchelder, N. T. Brewer, L. Cartegni, J. H. Hamilton, J. K. Hwang, S. H. Liu, S. V. Ilyushkin, C. Jost, M. Karny, A. Korgul, W. Królas, A. Kuźniak *et al.*, New half-lives of r -process Zn and Ga isotopes measured with electromagnetic separation, *Phys. Rev. Lett.* **109**, 112501 (2012).
- [10] P. T. Hosmer, H. Schatz, A. Aprahamian, O. Arndt, R. R. C. Clement, A. Estrade, K.-L. Kratz, S. N. Liddick, P. F. Mantica, W. F. Mueller, F. Montes, A. C. Morton, M. Ouellette, E. Pellegrini, B. Pfeiffer, P. Reeder, P. Santi, M. Steiner, A. Stolz, B. E. Tomlin *et al.*, Half-life of the doubly magic r -process nucleus ^{78}Ni , *Phys. Rev. Lett.* **94**, 112501 (2005).
- [11] M. Quinn, A. Aprahamian, J. Pereira, R. Surman, O. Arndt, T. Baumann, A. Becerril, T. Elliot, A. Estrade, D. Galaviz, T. Ginter, M. Hausmann, S. Hennrich, R. Kessler, K.-L. Kratz, G. Lorusso, P. F. Mantica, M. Matos, F. Montes, B. Pfeiffer *et al.*, β decay of nuclei around ^{90}Se : Search for signatures of a $N = 56$ subshell closure relevant to the r process, *Phys. Rev. C* **85**, 035807 (2012).
- [12] P. Hosmer, H. Schatz, A. Aprahamian, O. Arndt, R. R. C. Clement, A. Estrade, K. Farouqi, K.-L. Kratz, S. N. Liddick, A. F. Lisetskiy, P. F. Mantica, P. Möller, W. F. Mueller, F. Montes, A. C. Morton, M. Ouellette, E. Pellegrini, J. Pereira, B. Pfeiffer, P. Reeder *et al.*, Half-lives and branchings for β -delayed neutron emission for neutron-rich Co–Cu isotopes in the r -process, *Phys. Rev. C* **82**, 025806 (2010).
- [13] F. Montes, A. Estrade, P. T. Hosmer, S. N. Liddick, P. F. Mantica, A. C. Morton, W. F. Mueller, M. Ouellette, E. Pellegrini, P. Santi, H. Schatz, A. Stolz, B. E. Tomlin, O. Arndt, K.-L. Kratz, B. Pfeiffer, P. Reeder, W. B. Walters, A. Aprahamian, and A. Wöhr, β -decay half-lives and β -delayed neutron emission probabilities for neutron rich nuclei close to the $N = 82r$ -process path, *Phys. Rev. C* **73**, 035801 (2006).
- [14] I. Dillmann, K.-L. Kratz, A. Wöhr, O. Arndt, B. A. Brown, P. Hoff, M. Hjorth-Jensen, U. Köster, A. N. Ostrowski, B. Pfeiffer, D. Seweryniak, J. Shergur, and W. B. Walters (the ISOLDE Collaboration), $N = 82$ shell quenching of the classical r -process “waiting-point” nucleus ^{130}Cd , *Phys. Rev. Lett.* **91**, 162503 (2003).
- [15] G. Lorusso, S. Nishimura, Z. Y. Xu, A. Jungclaus, Y. Shimizu, G. S. Simpson, P.-A. Söderström, H. Watanabe, F. Browne, P. Doornenbal, G. Gey, H. S. Jung, B. Meyer, T. Sumikama, J. Taprogge, Z. Vajta, J. Wu, H. Baba, G. Benzoni, K. Y. Chae *et al.*, β -decay half-lives of 110 neutron-rich nuclei across the $N = 82$ shell gap: Implications for the mechanism and universality of the astrophysical r process, *Phys. Rev. Lett.* **114**, 192501 (2015).
- [16] S. Nishimura, Z. Li, H. Watanabe, K. Yoshinaga, T. Sumikama, T. Tachibana, K. Yamaguchi, M. Kurata-Nishimura, G. Lorusso, Y. Miyashita, A. Odahara, H. Baba, J. S. Berryman, N. Blasi, A. Bracco, F. Camera, J. Chiba, P. Doornenbal, S. Go, T. Hashimoto *et al.*, β -decay half-lives of very neutron-rich Kr to Tc isotopes on the boundary of the r -process path: An indication of fast r -matter flow, *Phys. Rev. Lett.* **106**, 052502 (2011).
- [17] A. I. Morales, J. Benlliure, T. Kurtukián-Nieto, K.-H. Schmidt, S. Verma, P. H. Regan, Z. Podolyák, M. Górska, S. Pietri, R. Kumar, E. Casarejos, N. Al-Dahan, A. Algora, N. Alkhamashi, H. Álvarez-Pol, G. Benzoni, A. Blazhev, P. Boutachkov, A. M. Bruce, L. S. Cáceres *et al.*, Half-life systematics across the $N = 126$ shell closure: Role of first-forbidden transitions in the β decay of heavy neutron-rich nuclei, *Phys. Rev. Lett.* **113**, 022702 (2014).
- [18] R. Caballero-Folch, C. Domingo-Pardo, J. Agramunt, A. Algora, F. Ameil, Y. Ayyad, J. Benlliure, M. Bowry, F. Calviño, D. Cano-Ott, G. Cortès, T. Davinson, I. Dillmann, A. Estrade, A. Evdokimov, T. Faestermann, F. Farinon, D. Galaviz, A. R. García, H. Geissel *et al.*, β -decay half-lives and β -delayed neutron emission probabilities for several isotopes of Au, Hg,

- Tl, Pb, and Bi, beyond $N = 126$, *Phys. Rev. C* **95**, 064322 (2017).
- [19] Y. X. Watanabe, Y. H. Kim, S. C. Jeong, Y. Hirayama, N. Imai, H. Ishiyama, H. S. Jung, H. Miyatake, S. Choi, J. S. Song, E. Clement, G. de France, A. Navin, M. Rejmund, C. Schmitt, G. Pollarolo, L. Corradi, E. Fioretto, D. Montanari, M. Niiikura *et al.*, Pathway for the production of neutron-rich isotopes around the $N = 126$ shell closure, *Phys. Rev. Lett.* **115**, 172503 (2015).
- [20] Y. Hirayama, H. Miyatake, Y. X. Watanabe, N. Imai, H. Ishiyama, S. C. Jeong, H. S. Jung, M. Oyaizu, M. Mukai, S. Kimura, T. Sonoda, M. Wada, Y. H. Kim, M. Huyse, Yu. Kudryavtsev, and P. Van Duppen, Beta-decay spectroscopy of r -process nuclei around $N = 126$, *EPJ Web Conf.* **109**, 08001 (2016).
- [21] P. Möller, J. Nix, and K.-L. Kratz, Nuclear properties for astrophysical and radioactive-ion-beam applications, *At. Data Nucl. Data Tables* **66**, 131 (1997).
- [22] P. Möller, M. Mumpower, T. Kawano, and W. Myers, Nuclear properties for astrophysical and radioactive-ion-beam applications (II), *At. Data Nucl. Data Tables* **125**, 1 (2019).
- [23] P. Möller, B. Pfeiffer, and K.-L. Kratz, New calculations of gross β -decay properties for astrophysical applications: Speeding-up the classical r process, *Phys. Rev. C* **67**, 055802 (2003).
- [24] J. Engel, M. Bender, J. Dobaczewski, W. Nazarewicz, and R. Surman, β decay rates of r -process waiting-point nuclei in a self-consistent approach, *Phys. Rev. C* **60**, 014302 (1999).
- [25] D.-L. Fang, B. A. Brown, and T. Suzuki, Investigating β -decay properties of spherical nuclei along the possible r -process path, *Phys. Rev. C* **88**, 034304 (2013).
- [26] I. N. Borzov, Gamow-Teller and first-forbidden decays near the r -process paths at $N = 50, 82$, and 126 , *Phys. Rev. C* **67**, 025802 (2003).
- [27] T. Marketin, L. Huther, and G. Martínez-Pinedo, Large-scale evaluation of β -decay rates of r -process nuclei with the inclusion of first-forbidden transitions, *Phys. Rev. C* **93**, 025805 (2016).
- [28] M. T. Mustonen and J. Engel, Global description of β^- decay in even-even nuclei with the axially-deformed Skyrme finite-amplitude method, *Phys. Rev. C* **93**, 014304 (2016).
- [29] E. M. Ney, J. Engel, T. Li, and N. Schunck, Global description of β^- decay with the axially deformed Skyrme finite-amplitude method: Extension to odd-mass and odd-odd nuclei, *Phys. Rev. C* **102**, 034326 (2020).
- [30] Z. M. Niu, H. Z. Liang, B. H. Sun, W. H. Long, and Y. F. Niu, Predictions of nuclear β -decay half-lives with machine learning and their impact on r -process nucleosynthesis, *Phys. Rev. C* **99**, 064307 (2019).
- [31] C. E. P. Robin and G. Martínez-Pinedo, Competition between allowed and first-forbidden β decay in r -process waiting-point nuclei within a relativistic beyond-mean-field approach, [arXiv:2403.17115](https://arxiv.org/abs/2403.17115).
- [32] K. Langanke and G. Martínez-Pinedo, Nuclear weak-interaction processes in stars, *Rev. Mod. Phys.* **75**, 819 (2003).
- [33] G. Martínez-Pinedo, Weak interaction rates in astrophysics, *Nucl. Phys. A* **688**, 357 (2001).
- [34] T. Suzuki, T. Yoshida, T. Kajino, and T. Otsuka, β decays of isotones with neutron magic number of $N = 126$ and r -process nucleosynthesis, *Phys. Rev. C* **85**, 015802 (2012).
- [35] Q. Zhi, E. Caurier, J. J. Cuenca-García, K. Langanke, G. Martínez-Pinedo, and K. Sieja, Shell-model half-lives including first-forbidden contributions for r -process waiting-point nuclei, *Phys. Rev. C* **87**, 025803 (2013).
- [36] T. Suzuki, S. Shibagaki, T. Yoshida, T. Kajino, and T. Otsuka, β -decay rates for exotic nuclei and r -process nucleosynthesis up to thorium and uranium, *Astrophys. J.* **859**, 133 (2018).
- [37] S. Sharma, P. C. Srivastava, A. Kumar, and T. Suzuki, Shell-model description for the properties of the forbidden β^- decay in the region “northeast” of ^{208}Pb , *Phys. Rev. C* **106**, 024333 (2022).
- [38] S. Sharma, P. C. Srivastava, A. Kumar, T. Suzuki, C. Yuan, and N. Shimizu, Shell-model study for allowed and forbidden β -decay properties in the “south” region of ^{208}Pb , [arXiv:2309.07903](https://arxiv.org/abs/2309.07903).
- [39] N. Shimizu, T. Togashi, and Y. Utsuno, Gamow-Teller transitions of neutron-rich $N = 82, 81$ nuclei by shell-model calculations, *Prog. Theor. Exp. Phys.* **2021**, 033D01 (2021).
- [40] H. Behrens and W. Bühring, *Electron Radial Wave Functions and Nuclear Beta-Decay*, International Series of Monographs on Physics (Clarendon Press, Oxford, 1982).
- [41] H. F. Schopper, *Weak Interactions and Nuclear Beta Decay* (North-Holland, Amsterdam, 1966).
- [42] S. Yoshida, Y. Utsuno, N. Shimizu, and T. Otsuka, Systematic shell-model study of β -decay properties and Gamow-Teller strength distributions in $A \approx 40$ neutron-rich nuclei, *Phys. Rev. C* **97**, 054321 (2018).
- [43] J. C. Hardy and I. S. Towner, Superaligned $0^+ \rightarrow 0^+$ nuclear β decays: A new survey with precision tests of the conserved vector current hypothesis and the standard model, *Phys. Rev. C* **79**, 055502 (2009).
- [44] J. Beringer *et al.* (Particle Data Group), Review of particle physics, *Phys. Rev. D* **86**, 010001 (2012).
- [45] E. Warburton, J. Becker, B. Brown, and D. Millener, First-forbidden beta decay near $A = 40$, *Ann. Phys. (NY)* **187**, 471 (1988).
- [46] M. Antony, A. Pape, and J. Britz, Coulomb displacement energies between analog levels for $3 \leq A \leq 239$, *At. Data Nucl. Data Tables* **66**, 1 (1997).
- [47] C. Yuan, M. Liu, N. Shimizu, Z. Podolyák, T. Suzuki, T. Otsuka, and Z. Liu, Shell-model study on spectroscopic properties in the region “south” of ^{208}Pb , *Phys. Rev. C* **106**, 044314 (2022).
- [48] G. Herling and T. Kuo, Two-particle states in ^{210}Pb , ^{210}Bi and ^{210}Po with realistic forces, *Nucl. Phys. A* **181**, 113 (1972).
- [49] E. K. Warburton, First-forbidden β decay in the lead region and mesonic enhancement of the weak axial current, *Phys. Rev. C* **44**, 233 (1991).
- [50] C. Qi, L. Y. Jia, and G. J. Fu, Large-scale shell-model calculations on the spectroscopy of $N < 126$ Pb isotopes, *Phys. Rev. C* **94**, 014312 (2016).
- [51] J. Chen, M. Liu, C. Yuan, S. Chen, N. Shimizu, X. Sun, R. Xu, and Y. Tian, Shell-model-based investigation on level density of Xe and Ba isotopes, *Phys. Rev. C* **107**, 054306 (2023).
- [52] E. Caurier, G. Martínez-Pinedo, F. Nowack, A. Poves, and A. P. Zuker, The shell model as a unified view of nuclear structure, *Rev. Mod. Phys.* **77**, 427 (2005).
- [53] T. Otsuka, M. Honma, T. Mizusaki, N. Shimizu, and Y. Utsuno, Monte Carlo shell model for atomic nuclei, *Prog. Part. Nucl. Phys.* **47**, 319 (2001).

- [54] T. Otsuka, A. Gade, O. Sorlin, T. Suzuki, and Y. Utsuno, Evolution of shell structure in exotic nuclei, *Rev. Mod. Phys.* **92**, 015002 (2020).
- [55] B. Brown and B. Wildenthal, Experimental and theoretical Gamow-Teller beta-decay observables for the *sd*-shell nuclei, *At. Data Nucl. Data Tables* **33**, 347 (1985).
- [56] G. Martínez-Pinedo, A. Poves, E. Caurier, and A. P. Zuker, Effective g_A in the *pf* shell, *Phys. Rev. C* **53**, R2602 (1996).
- [57] A. Kumar, P. C. Srivastava, and T. Suzuki, Shell model results for nuclear β^- -decay properties of *sd*-shell nuclei, *Prog. Theor. Exp. Phys.* **2020**, 033D01 (2020).
- [58] J. T. Suhonen, Value of the axial-vector coupling strength in β and $\beta\beta$ decays: A review, *Front. Phys.* **5**, 55 (2017).
- [59] B. Singh, Nuclear data sheets for $A = 199$, *Nucl. Data Sheets* **108**, 79 (2007).
- [60] F. Kondev and S. Lalkovski, Nuclear data sheets for $A = 200$, *Nucl. Data Sheets* **108**, 1471 (2007).
- [61] L. Rydström, J. Blomqvist, R. Liotta, and C. Pomar, Structure of proton-deficient nuclei near ^{208}Pb , *Nucl. Phys. A* **512**, 217 (1990).
- [62] E. K. Warburton, Core polarization effects on spin-dipole and first-forbidden β -decay operators in the lead region, *Phys. Rev. C* **42**, 2479 (1990).
- [63] E. Warburton and I. Towner, Nuclear medium effects in first forbidden beta decay, *Phys. Rep.* **242**, 103 (1994).
- [64] N. Gove and M. Martin, Log- f tables for beta decay, *At. Data Nucl. Data Tables* **10**, 205 (1971).
- [65] F. Kondev, Nuclear data sheets for $A = 205$, *Nucl. Data Sheets* **166**, 1 (2020).
- [66] F. Kondev, Nuclear data sheets for $A = 206$, *Nucl. Data Sheets* **109**, 1527 (2008).
- [67] F. Kondev and S. Lalkovski, Nuclear data sheets for $A = 207$, *Nucl. Data Sheets* **112**, 707 (2011).
- [68] C. Wennemann, W. D. Schmidt-Ott, T. Hild, K. Krumbholz, V. Kunze, F. Meißner, H. Keller, R. Kirchner, and E. Roeckl, Investigation of new neutron-rich gold isotopes ^{203}Au and ^{205}Au , *Z. Phys. A: Hadrons Nucl.* **347**, 185 (1994).
- [69] G. F. Farrelly, Gamma and beta decay spectroscopy of ^{190}W , ^{205}Au and ^{203}Au , Ph.D. thesis, Surrey University, 2010.
- [70] Nuclear data center, japan atomic energy agency, estimation of beta-decay properties, <https://www.ndc.jaea.go.jp/nucldata/beta-decay-properties.pdf>.
- [71] T. Tachibana and M. Yamada, *Proceedings of International Conference on Exotic Nuclei and Atomic Masses, Arles, 1995*, edited by M. de Saint Simon and O. Sorlin (Editions Frontières, Gif-sur-Yvette, 1995), p. 763, and references therein; T. Yoshida and T. Tachibana, *J. Nucl. Sci. Technol.* **37**, 491 (2000); T. Tachibana, RIKEN Review, Focused on Models and Theories of the Nuclear Mass, **26**, 109 (2000).
- [72] H. Koura, T. Tachibana, M. Uno, and M. Yamada, Nuclidic mass formula on a spherical basis with an improved even-odd term, *Prog. Theor. Phys.* **113**, 305 (2005).
- [73] R. R. Whitehead, Moment methods and lanczos methods, in *Theory and Applications of Moment Methods in Many-Fermion Systems*, edited by B. J. Dalton, S. M. Grimes, J. D. Vary, and S. A. Williams (Plenum, New York, 1980), p. 235.
- [74] Y. Utsuno, N. Shimizu, T. Otsuka, S. Ebata, and M. Honma, Photonuclear reactions of calcium isotopes calculated with the nuclear shell model, *Prog. Nucl. Energy* **82**, 102 (2015).
- [75] Nudat 3.0, <https://www.nndc.bnl.gov/nudat3/>.
- [76] T. Otsuka, T. Suzuki, M. Honma, Y. Utsuno, N. Tsunoda, K. Tsukiyama, and M. Hjorth-Jensen, Novel features of nuclear forces and shell evolution in exotic nuclei, *Phys. Rev. Lett.* **104**, 012501 (2010).
- [77] S. P. Pandya, Nucleon-hole interaction in *jj* coupling, *Phys. Rev.* **103**, 956 (1956).
- [78] K. L. G. Heyde, *The Nuclear Shell Model*, 2nd ed. (Springer, Berlin, 1994), Sec. 3.4.3.
- [79] N. Shimizu, T. Mizusaki, Y. Utsuno, and Y. Tsunoda, Thick-restart block Lanczos method for large-scale shell-model calculations, *Comput. Phys. Commun.* **244**, 372 (2019).